communications earth & environment

Article

A Nature Portfolio journal

https://doi.org/10.1038/s43247-025-02366-2

Antarctic Ice Sheet tipping in the last 800,000 years warns of future ice loss

Check for updates

David M. Chandler[1] ✉, Petra M. Langebroek[1], Ronja Reese[2], Torsten Albrecht[3,4], Julius Garbe[3,5] & Ricarda Winkelmann[3,4,5]

Ice loss from Antarctica's vast freshwater reservoir could threaten coastal communities and the global economy if the ice volume decreases by just a few percent. Observed changes in mass balance are limited to ~40 years, and are difficult to interpret in the context of an ice sheet with response time scales reaching centuries to millennia. To gain a much longer-term perspective, here we combine transient and equilibrium Parallel Ice Sheet Model simulations of Antarctic Ice Sheet response to glacial-interglacial warming and cooling cycles over the last 800,000 years. We find hysteresis that is caused by the long response time and by crossing of tipping points. Notably, West Antarctic Ice Sheet collapse contributes over 4 m sea-level rise in equilibrium ice sheet states with little (0.25 °C) or even no ocean warming above present. Therefore, today we are likely already at (or almost at) an overshoot scenario, supporting recent studies warning of substantial irreversible ice loss with little or no further climate warming.

The Antarctic Ice Sheet holds by far the greatest sea-level rise potential (~58 m[1]), and its contribution to future sea-level rise constitutes one of the highest uncertainties in projections[2,3]. This uncertainty reflects diverging projections of climatic boundary conditions, and difficulties in estimating how ice dynamic processes might modify the balance between ocean-driven mass losses and interior mass gains[2–4]. Poorly-constrained Antarctic ice loss itself contributes further uncertainty in climate projections, due to the global impacts of freshwater discharge into the Southern Ocean[5–7] and interactions with other parts of the Earth system, in particular other tipping elements and tipping cascades[8,9]. A key question for both sea-level and climate projections is the risk of triggering dynamic instabilities. In particular, the marine ice sheet and marine ice cliff instabilities (MISI and MICI) in sectors of Antarctica currently grounded below sea-level could contribute several metres of sea-level rise[2,10,11].

Simulated ice sheet responses to warm periods in the geological past can help to disentangle the different sources of uncertainty and better inform future projections. Their unknown initial states, estimated (reconstructed) boundary conditions, and known (observed present-day) final state complement future scenarios which have an initial state constrained by available observations of ice geometry and surface velocity, projected boundary conditions, but unknown final state. The last interglacial has been widely used for this purpose[12–15]. However, ice sheet simulations over several glacial cycles[16–19]—some a little cooler or warmer than present[20]—can build a more consistent picture of temperature thresholds for instability, overshoots, and subsequent recovery, than can be obtained from simulating one glacial-interglacial cycle. None of these past studies has looked for tipping behaviour in ice sheet response.

Here we run transient and equilibrium Antarctic Ice Sheet simulations over the last 800 kyr (eight glacial cycles), forced by paleoclimate reconstructions, to identify temperature thresholds that could have triggered substantial (several metres) sea-level rise above present-day. We consider the reversibility of these sea-level changes and assess how both lagged responses and tipping points influence ice sheet response to climatic changes.

The Antarctic Ice Sheet is simulated with the Parallel Ice Sheet Model (PISM) v1.0[21,22]. We model ice sheet surface air temperature and precipitation changes using near-surface air temperature reconstructions[23,24] adjusted for elevation changes similarly to ref. 25. Deep ocean temperature changes are derived from Antarctic surface air temperatures using a linear response function (LRF)[25,26], validated for the study period by comparison with proxy reconstructions[27,28] (Methods and Fig. S1). Sea-level is imposed using a global mean sea-level (GMSL) reanalysis[29]. Further details are provided in the 'Methods'.

Transient ice sheet states were simulated by running PISM from 800 ka to present. Three different model configurations sampled parametric uncertainty (Runs A, B and C: Fig. 1, Table 1 and Methods). Equilibrium ice

[1]NORCE Research AS, Bjerknes Centre for Climate Research, Bergen, Norway. [2]Geography and Environmental Sciences, Northumbria University, Newcastle, UK. [3]Potsdam Institute for Climate Impact Research (PIK), Member of the Leibniz Association, Potsdam, Germany. [4]Integrative Earth System Science, Max Planck Institute of Geoanthropology, Jena, Germany. [5]Institute of Physics and Astronomy, University of Potsdam, Potsdam, Germany.
✉e-mail: dcha@norceresearch.no

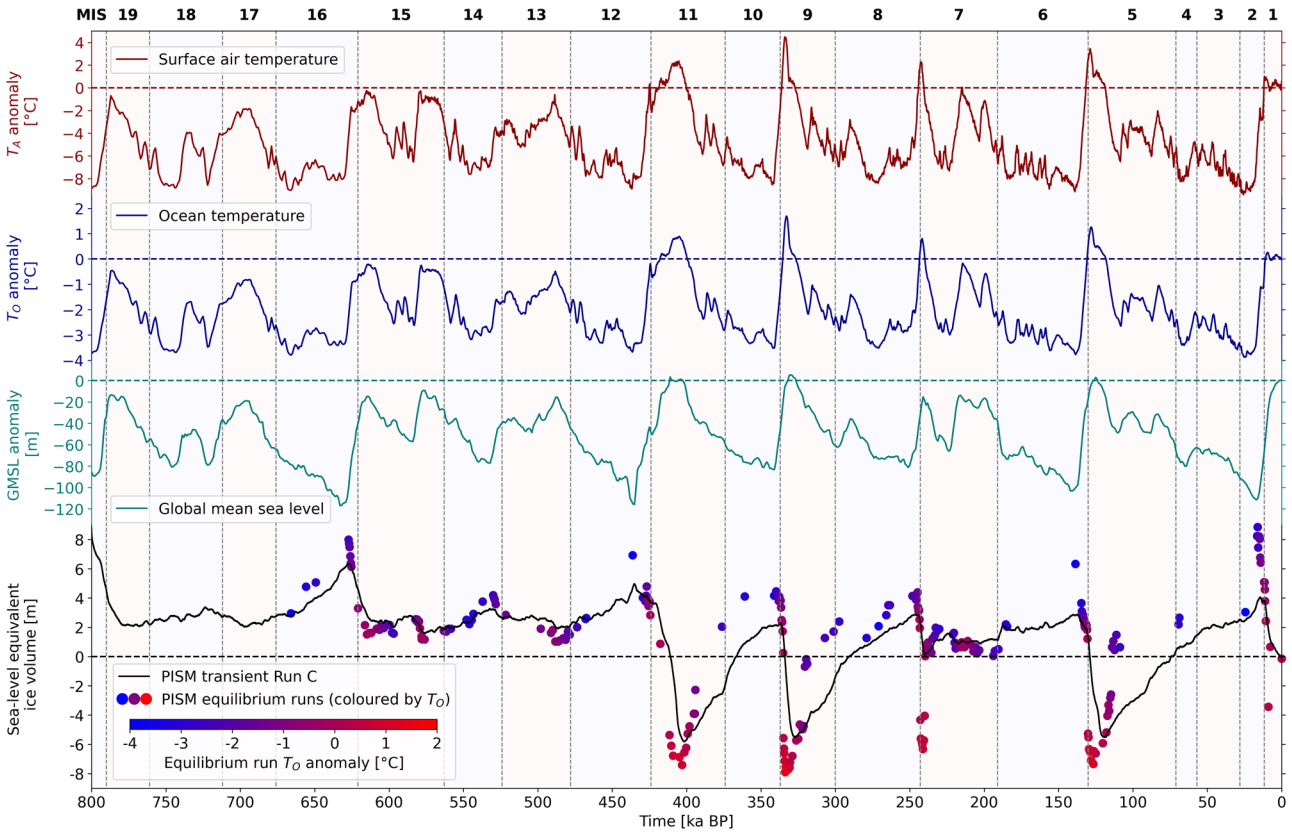

Fig. 1 | Glacial-interglacial surface temperature, ocean temperature and sea-level forcings, and resulting Antarctic Ice Sheet ice volume, for Run C. Surface air temperature (T_A anomaly) is reconstructed from five ice-cores[23,24,152] (see Methods). The ocean temperature forcing (T_O anomaly) is calculated from T_A, using a linear response function[25,26] (see Methods and Fig. S1 for validation). The global mean sea-level (GMSL) anomaly is a reanalysis of globally distributed reconstructions[29]. Simulated Antarctic Ice Sheet ice volumes are from transient Run C (black line) and respective quasi-equilibrium runs (circles, with colours showing the ocean temperature anomaly compared to present during the equilibrium run). Numbered vertical bands show marine isotope stages (odd-numbered interglacials; even-numbered glacials)[143].

Table 1 | PISM configuration in simulations by Albrecht et al.[25,93] (A2020: their recommended parameter choices), and in our three 800 kyr simulations (A, B and C, of which B and C were used for additional equilibrium runs)

Parameter	A2020	Run A	Run B	Run C	Description
E_{SIA}	2.0	2.0	1.5	1.8	Enhancement factor, SIA
E_{SSA}	0.60	0.80	0.80	0.60	Enhancement factor, SSA
q	0.75	0.33	0.33	0.33	Pseudo-plastic friction exponent
u_0	100	55	60	42	Threshold velocity [m s^{-1}]
ϕ_{min}, ϕ_{max}	–(*)	18, 33	20, 30	20, 30	topg-to-phi till friction angle range [°]
z_{min}, z_{max}	–(*)	−1000, −200	−1000, −200	−1000, −200	topg-to-phi bed elevation range [m]
δ	4.0	1.5	1.5	1.1	Lower limit on till water effective pressure [%]
C_d	1.0	5.0	3.0	1.5	Till water drainage rate [mm yr^{-1}]
W_{max}	2.0	2.0	2.0	1.0	Maximum equivalent water layer thickness in till [m]
η	5.0×10^{20}	5.0×10^{19}	5.0×10^{19}	5.0×10^{19}	Mantle viscosity [Pa s]
f_{prec}	7.0	5.0	4.4	6.0	Precipitation scaling factor [% K^{-1}]
PICO γ_T	1.00	0.43	0.40	0.90	Turbulent exchange velocity [10^{-5} m s^{-1}]
PICO C	0.8	12.9	15.0	20.6	Overturning coeff. [10^6 m^6 kg^{-1} s^{-1}]
H_{calv}	75	150	150	150	Thickness calving threshold [m]
K_{calv}	1.0	0.5	0.5	0.6	Eigencalving constant [10^{17} m s]
δT_O	LRF	LRF	As Run A	As Run A	Ocean temperature anomaly (method)
δT_{OPD}	S2014	WOA-18	WOA-18	WOA-18	Ocean temperature anomaly (modern reference)

Final states for Runs A, B and C are compared with present-day observations in Fig. S4. (*) A2020 used a spatially variable $2 \le \phi \le 70$ assigned in an inversion of surface velocity.
LRF linear response function (see Methods), S2014 Schmidtko et al.[34], *SIA* shallow ice approximation, *SSA* shallow shelf approximation, *WOA-18* World Ocean Atlas 2018[94].

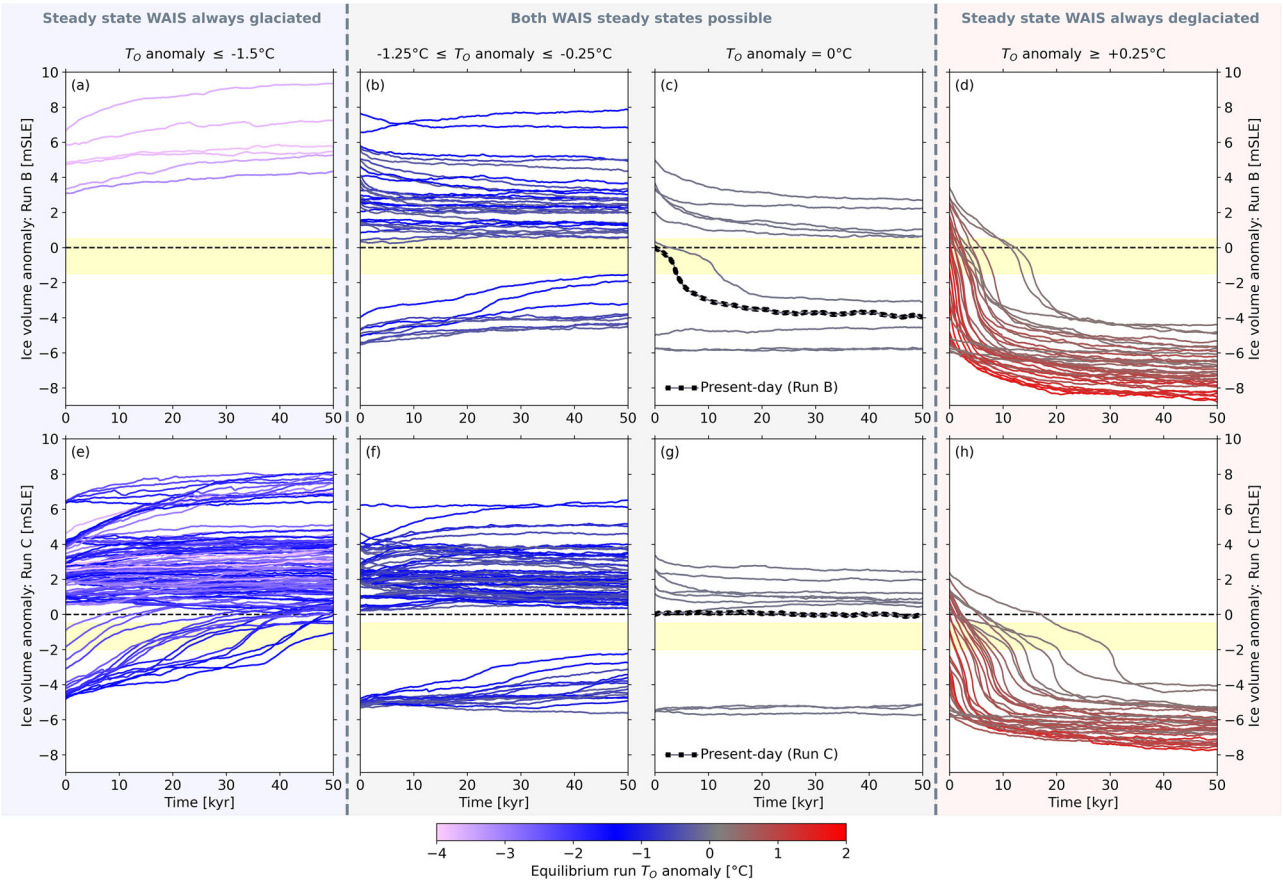

Fig. 2 | Evolution of the ice sheet from its transient to quasi-equilibrium states. The top row (Run B) and bottom row (Run C) are split into three cases based on ocean temperature anomaly T_O and corresponding ice sheet response. For $T_O \leq -1.5$ °C (**a**, **e**), West Antarctica always evolves towards a glaciated steady state *above* the yellow band. For $T_O \geq +0.25$ °C (**d**, **h**), West Antarctica always evolves towards a deglaciated steady state *below* the yellow band. At intermediate temperatures $-1.25 \leq T_O \leq 0$ °C (**b**, **c**, **f**, **g**) both glaciated and deglaciated steady states are possible. Equilibrium simulations starting from present-day are highlighted with black squares in (**c**, **g**). There are no steady states within the yellow band. Dashed vertical lines separating the three cases correspond to the glaciation and deglaciation tipping points at −1.5 to −1.25 °C and 0 to +0.25 °C, respectively.

sheet states in Runs B and C were then simulated by starting with snapshots from the transient run and integrating these forwards under constant climate and sea-level conditions equivalent to those at the time of the respective snapshot (Figs. 1, 2). These equilibrium simulations allow us to identify what stable states (if any) the ice sheet is evolving towards, for a range of given climate states. We can then distinguish whether hysteresis between climate forcing and simulated ice volume (Figs. 3, S2) is due to tipping points or simply a lagged response. In the former case, multi-stability causes path-dependent steady states; in the latter case there is only one, path-independent, steady state[12,30].

Results and discussion

Transient and equilibrium ice sheet states

Transient ice sheet states during relatively cool interglacials up to marine isotope stage (MIS) 13 remain within ~2 m sea-level equivalent (SLE) of their equilibrium ice volume (Figs. 1, 3a, d). In contrast, transient responses to the stronger glacial cycles since MIS 12 evolve far (over 8 m SLE) from equilibrium, particularly during interglacials (Figs. 1, 3b, c,e, f). In these warmer interglacials, hysteresis in both equilibrium states and transient states (Fig. 3c, f) shows that the transient response derives primarily from internal instability, or tipping points, rather than a lagged response to external forcing. A deglaciation tipping point occurs consistently in the equilibrium simulations for both configurations B and C at ocean temperature anomalies of 0 to +0.25 °C compared to present (Figs. 3, S2), indicating a persistent ocean temperature threshold through at least the last eight glacial cycles. On the upper hysteresis branch (Fig. 3c, f), crossing of the deglaciation tipping point triggers collapse of all three main marine basins in the West Antarctic Ice Sheet (WAIS), but there is little retreat in East Antarctica (Fig. 4). The long response time keeps the ice sheet on the upper branch for up to 2 kyr even after the ocean temperature threshold has been crossed.

Once on the lower branch, WAIS recovery by tipping back to the upper branch occurs only once the ocean temperature cools between −1.25 and −1.5 °C below present (Figs. 3c, f, 4). Transition to the upper branch is much slower than the deglaciation phase, typically taking over 10 kyr. Note that with our optimisation targets and anomaly-based forcing, we have less confidence in our simulations under increasingly cold climates - for example, due to potential changes in atmospheric or ocean circulation in a glacial climate state (e.g. ref. 31) that are not captured by our approach (see Methods).

Importantly, WAIS tips to (or remains in) its retreated state in all equilibrium simulations with ocean temperatures warmer than present - as well as in the equilibrium runs with present-day climate in Runs A and B (Figs. 2, 4, S2). The ice sheet remains in its retreated state when the ocean cools back to present-day conditions, highlighting the effective irreversibility of WAIS collapse and the corresponding sea-level rise in a climate policy and planning context. However, both the duration and magnitude of interglacial warming are important factors for triggering tipping in transient states. This is illustrated by interglacial MIS 7, where warming is *sufficiently strong* to trigger tipping and WAIS ice loss in equilibrium states (Fig. 3b, e)

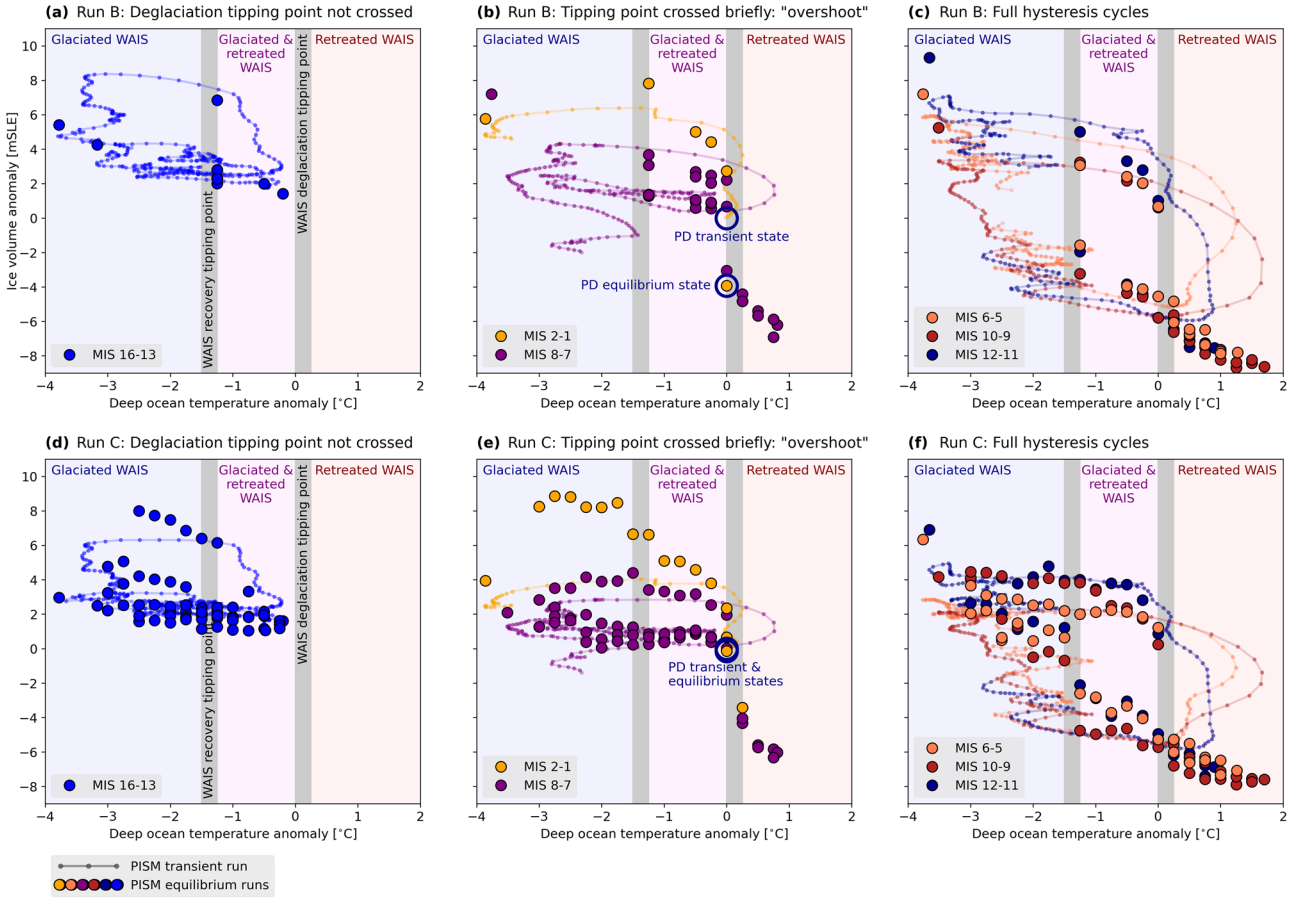

Fig. 3 | Relationship between ocean forcing and grounded ice sheet volume, with hysteresis and tipping points emerging in warmer interglacials. The PISM transient states (line coloured by marine isotope stage: MIS) are marked with small circles every 500 years. Equilibrium ice volume (larger circles) is coloured by the respective marine isotope stage (MIS). Three different behaviours are identified in glacial cycles. **a**, **d**: no substantial retreat of the West Antarctic Ice Sheet (WAIS) in either the transient or equilibrium states. **b**, **e**: an overshoot scenario where interglacial conditions are sufficiently warm to *briefly* cross the WAIS deglaciation tipping point (0 to +0.25 °C), triggering WAIS collapse in the equilibrium state but not in the transient state. The present-day interglacial (MIS 1) fits this scenario. **c**, **f**: sufficiently sustained interglacial warming to trigger WAIS collapse in both the transient and equilibrium states. Recovery of WAIS is triggered at ocean temperature anomalies below −1.25 °C; consequently ice sheet states are multi-stable between the WAIS recovery and deglaciation tipping points. The dominant contribution of WAIS to this hysteresis is evident in Fig. 4. Complete hysteresis plots for the full 800 kyr are shown in Fig. S2.

but is *insufficiently sustained* to trigger tipping during the transient run. This overshoot scenario best represents our present-day ice sheet in Runs A and B (Figs. 3b, S2a,b), indicating we have likely crossed the temperature threshold for WAIS collapse, but not yet for long enough, similar to a recent ensemble-based experiment[32,33]. In Run C we would cross the tipping point with less than 0.25°C ocean warming (Figs. 3e, S2c), likely within the next few decades according to recent deep ocean warming rates close to Antarctica[34,35].

Comparison with geological evidence for instability

Geological evidence for the extent of WAIS collapse during Pleistocene interglacials has remained ambiguous: although marine sedimentary geochemical and fossil archives clearly indicate periods of WAIS retreat[36–41], these cannot yet quantify the maximum extent of retreat. Ice core oxygen isotopic records are similarly inconclusive[42–44]. Analysis of blue ice areas[13] and octopus genomic evidence[45] adds support for full collapse, at least during the last interglacial. This would be consistent with our three transient runs A-C. Finally, a sea salt sodium record extracted from Skytrain Ice Rise[46] indicates the Ronne Ice Shelf may have persisted through the last interglacial, in contrast to our simulated loss of ice shelves in the Weddell Sea sector.

The East Antarctic ice core record[24], and radiostratigraphy[47], testify to this region's stability for several glacial cycles, at least in the interior. Response of the Wilkes and Aurora basins of East Antarctica to interglacial warming is less certain, but is an important question: these basins are extensively grounded below sea-level, and their collapse (via the marine ice sheet instability, similarly to West Antarctica) could yield several metres of sea-level rise. Substantial interglacial ice loss from the Wilkes basin has been suggested[48–50], but the evidence hinges on inferred thinning at Talos Dome[50] and a detrital ϵ_{Nd} record in sediment core U1361[49] on the continental rise some 600–700 km from the present-day Mertz and Ninnis grounding lines. This evidence is not necessarily consistent with extensive interglacial retreat of the Wilkes basin[15,51,52]. Similarly to other recent ice sheet simulations[15,17–19] we find no collapse of the East Antarctic marine basins since 800 ka. The evolution of this region in recent interglacials remains an open question pending more direct geological or proxy evidence.

Our peak Antarctic Ice Sheet contributions of ~5 m SLE during interglacials 11, 9 and 5 are reasonably consistent with the imposed GMSL reconstruction of +3–5 m[29] (which is not inevitable, given the flexibility in modelling choices). They are also within the uncertainty range of an estimated Antarctic last interglacial sea-level contribution of 3.6–8.7 m[53]. Therefore, we find WAIS collapse is alone sufficient to explain sea-level reconstructions, without needing a substantial additional contribution from EAIS retreat. Overall, our simulations indicate an intermittent West Antarctic and probably stable East Antarctic ice sheet during recent interglacials with relatively modest ocean warming in comparison to IPCC projections[54].

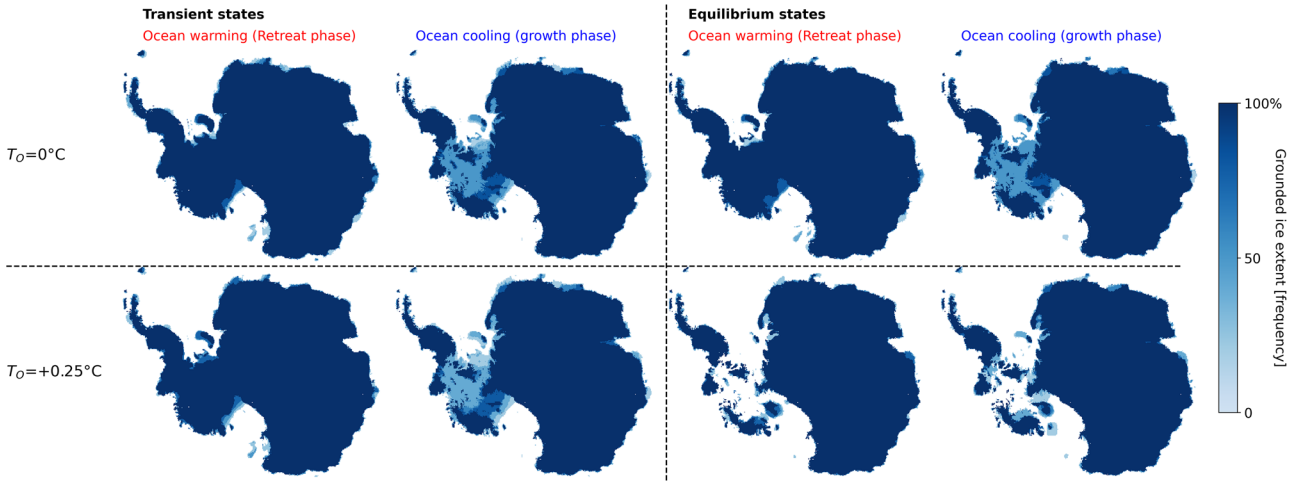

Fig. 4 | Grounded ice sheet extent in transient Run C and corresponding equilibrium states for ocean temperatures close to present-day. Darker shading indicates grounded ice in greater proportions of transient run snapshots (left plots) or equilibrium states (right plots). The top row is for present-day ocean temperature, and the bottom row for a slightly warmer ocean (T_0 = +0.25 °C). Ice sheet extents demonstrate clear path-dependence, with generally greater grounded ice areas in the warming phase than in the cooling phase, for a given ocean temperature.

Ocean temperature control on tipping

Strong correlation between ocean temperature (T_O) and the other two forcings (air temperature T_A, and GMSL: Fig. 1) potentially complicates attribution of the tipping behaviour directly to T_O. Under warming reconstructed in our study period ($T_A < +5$ °C), and similar to ref. 55, ice loss remains driven primarily by calving and ice shelf basal melt (Fig. S1)—neither of which are directly air-temperature dependent in our model setup (we do not explicitly model ice shelf hydrofracture: see below). Therefore, we can at least exclude air temperature as the primary trigger for these tipping points. Sea-level is harder to separate as it influences grounding line positions, and in turn the ice shelf cavity geometry and sub-shelf melting, ultimately impacting on upstream grounded ice dynamics. However, when examining the transitions from the upper to lower hysteresis branches in the equilibrium simulations (Figs. 3, 5), we find tipping occurs consistently at 0 to +0.25 °C but at less consistent GMSL. For example in Run B: tipping occurred at −25 to −16 m GMSL in MIS 7 and 5, and at −11 to −1 m GMSL in MIS 9; but no tipping occurred in equilibrium runs at sea-levels of −14 or −19 m in MIS 13 and 15, respectively. Hence, the tipping behaviour appears most strongly associated with T_O.

The influence of ocean temperature is evident through the resulting changes in ice shelf basal melting—in particular, the rapid increase in ice shelf basal melt in contrast to decreasing calving, as ocean temperature warms above present-day (Fig. 6).

Can missing feedbacks bias stability?

Modelling the Antarctic Ice Sheet over such long time scales requires inevitable compromises in resolution and the complexity of parameterisations[25], and precludes empirical (e.g. Monte-Carlo) uncertainty analysis that fully samples the parameter space (see Methods). Here we consider whether missing feedbacks might bias ice sheet stability in our simulations.

PISM does not model MICI and related feedbacks due to ice shelf hydrofracture[11]. Whether these processes reinforce instability in marine-based sectors remains debated[4]. Either way, including these processes is unlikely to alter our assessment of the present-day ice sheet state: this is because MICI is not likely underway at present[11], yet we find a sustained present-day climate is already sufficient (or very nearly sufficient) to trigger WAIS collapse (Figs. 2, 3). Hence, even if instability reinforced by MICI could accelerate ice loss and reduce borrowed time, it would not lower the ocean temperature threshold for tipping in the warming phase—this already occurs *before* there is sufficient surface melting to trigger MICI. Likewise, in the cooling phase MICI would not impact tipping to the upper hysteresis branch, as this transition occurs during cold climates with negligible surface melting and thus an absence of hydrofracturing.

Besides MICI, surface runoff and hydrofracturing can also influence grounded ice dynamics, by driving seasonal variations in subglacial water pressure and basal motion[56,57]. Hydrofracturing could further reduce ice viscosity and increase velocity, via deep latent heat release (cryohydrologic warming[58,59]). Seasonal melt-induced velocity variability is not observed under present-day conditions in Antarctica, except on the Peninsula[60], so our omission of related processes does not bias assessed present-day stability. However, the warmer interglacials 11, 9 and 5 (Fig. S1) may have driven more extensive surface melt and runoff. The question of whether runoff over such thick ice could accelerate dynamic ice loss (again, reducing borrowed time) remains open.

Changes in ocean circulation impact access of warm water masses to sub-shelf cavities (see Methods for further discussion). We also neglect feedbacks related to freshwater discharge, in which increased melt inputs likely strengthen ocean stratification that in turn causes surface cooling and warming at depth[5,6,61]. This process might accelerate ice shelf retreat[61], but can only be captured in detail by a coupled ice-ocean model. As increasing coupled model simulations become available we may in future be able to develop parameterisations that can modify the imposed ocean temperature forcing according to simulated ice shelf basal melt rates. Nevertheless, we here find that WAIS collapse occurs when ocean temperatures are at (Runs A, B) or within 0.25 °C (Run C) of their observed reference values, i.e., when uncertainties related to ocean circulation changes are minimal.

Finally, loss of WAIS considerably changes the configuration of the Antarctic coastline, in particular by opening deep connections between the Amundsen, Ross and Weddell seas (evident in Fig. 4). These seaways are not open at present so their potential influence on ocean circulation again does not impact our assessed stability of the present-day ice sheet state. However, the seaways presumably influence the recovery phase. Similarly, the climatic impacts of WAIS loss (for example, related to surface albedo or to changing surface topography) could increasingly affect WAIS ice loss as retreat progresses, or (more likely) during the recovery phase. These questions will need answering with additional climate or coupled climate-ice-sheet modelling experiments in future.

A warning from past persistence

Hysteresis cycles follow very similar trajectories through the warm interglacials 5, 9 and 11 in the three transient simulations (Figs. 3c, f, 6),

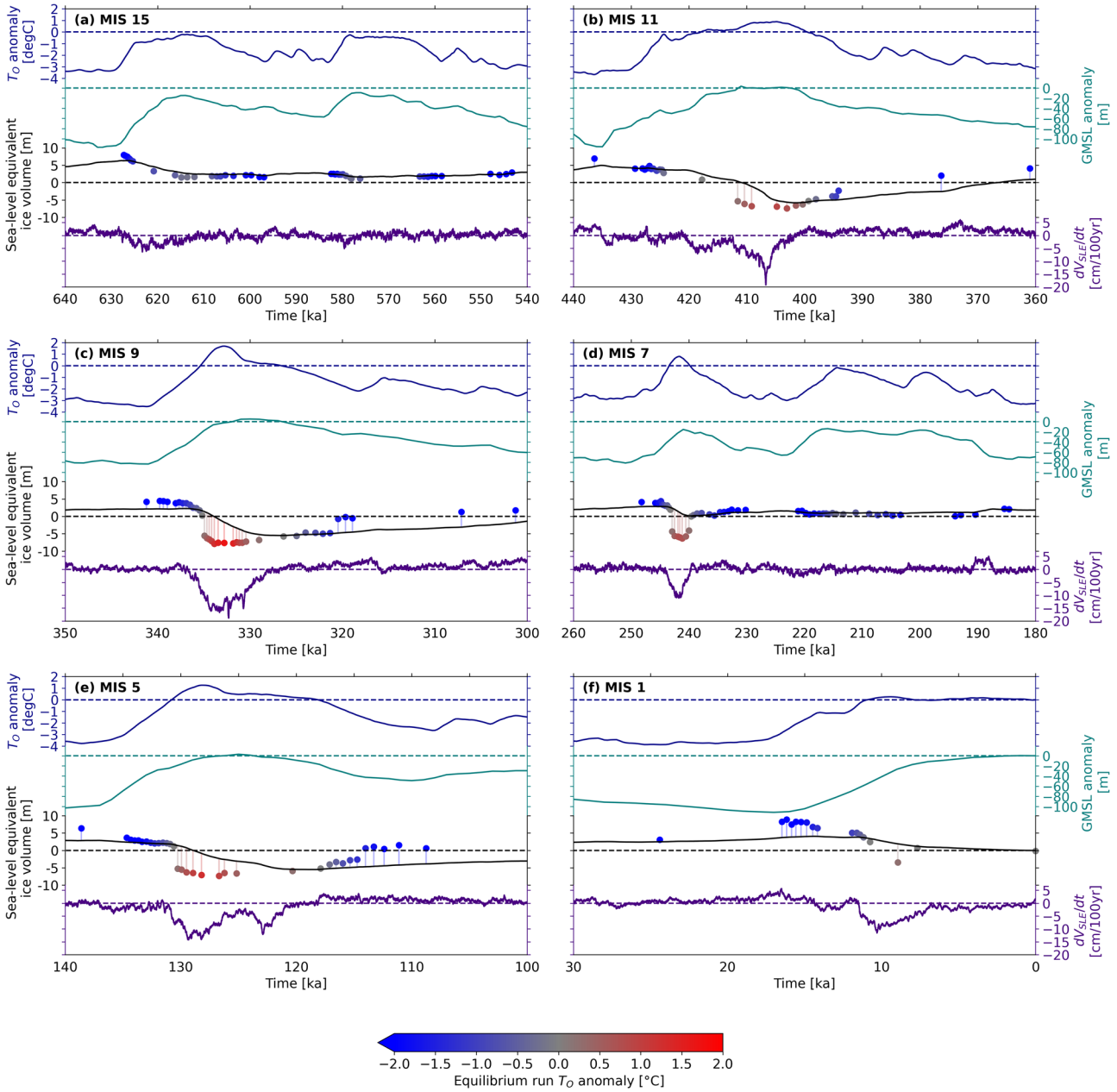

Fig. 5 | Ice sheet response to temperature and global mean sea-level (GMSL) changes in the relatively warmer interglacials. a–f show interglacials 15, 11, 9, 7, 5 and 1, respectively. Ocean temperature and GMSL forcings follow Fig. 1; ice sheet response in the PISM transient Run C is shown as the black line, and corresponding equilibrium states (circles) are coloured by ocean temperature. Rate of change of SLE ice volume (dV_{SLE}/dt) is shown in purple. Initial increases in deglacial ice loss correspond to continent-wide grounding line retreat towards their present-day locations. Distinct spikes in dV_{SLE}/dt reaching an equivalent 20 cm/century sea-level rise are associated with collapse of the Amundsen Sea and Weddell Sea sectors in MIS 11 at 408 ka; MIS 9 at 333–300 ka; and MIS 5 at 123 ka.

while respective equilibrium states are tightly clustered on both upper and lower branches (Fig. 3c, f) and have similar ice extents (Fig. 4). The temperature thresholds for tipping are consistent across all interglacials in all three configurations. This consistency, despite clear differences in the boundary conditions through each cycle (e.g., with respect to interglacial duration and magnitude: Fig. 1 and ref. 20), indicates some underlying predictability that provides strong support for Quaternary interglacials in informing estimates of future changes. It also provides confidence that our thresholds are a property of the ice sheet itself, without strong sensitivity to climate forcing uncertainties. This leads us to three main conclusions as follows.

First, we reiterate our view that the Antarctic Ice Sheet is presently in (or very close to) an overshoot state, which will tip to a retreated West Antarctic state contributing 4 m sea-level rise with little (<0.25 °C) or even no deep ocean warming (Fig. 3). 0.25 °C warming is likely within 50 years[34,35] even without additional carbon emissions. This supports other studies finding WAIS collapse without additional warming, using PISM[15,33] or other ice sheet models[62,63]. Tipping might not yet be inevitable (similar to refs. 32,33) and the time scale for full retreat of WAIS could be millennia (Fig. 2). However, this time scale may be drastically reduced by additional feedbacks discussed above, as well as by additional warming. Constraining the period of borrowed time before tipping will require improvements in our understanding and numerical representation of how ice-ocean and ice dynamic feedbacks in critical regions of Antarctica will control ice sheet response to projected warming scenarios. Additional paleo records from MIS 7 could provide further useful constraints: in our simulations this was

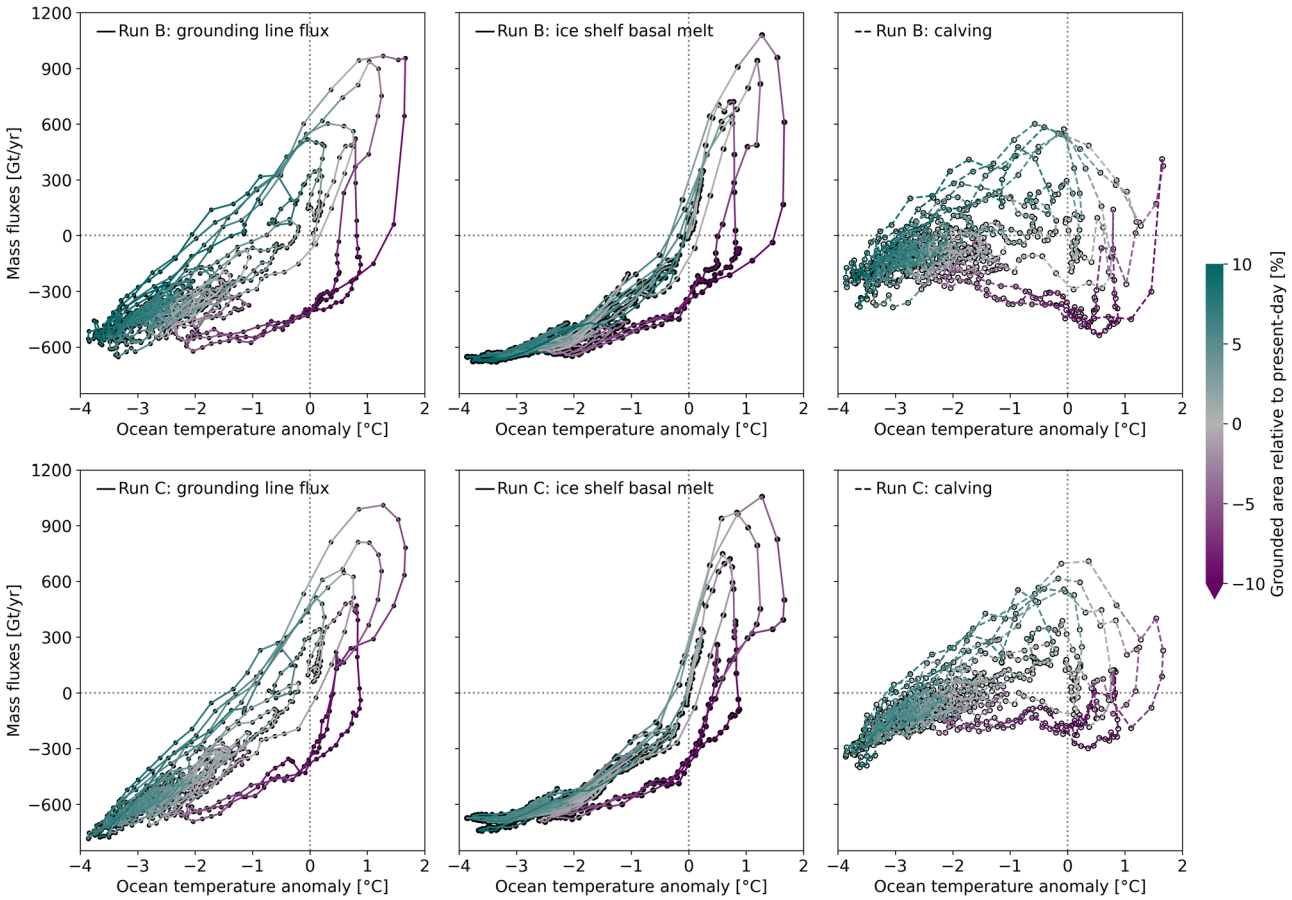

Fig. 6 | Grounding line, ice shelf basal melt and calving fluxes in transient runs B and C during MIS 12 to present. Lines are coloured by grounded ice extent and marked every 500 years. In each case, hysteresis is clockwise. Starting in a cold (glacial) ocean state, fluxes all increase with increasing ocean temperature while the West Antarctic Ice Sheet (WAIS) remains in its glaciated state (green shading). At ocean temperatures close to present-day, calving fluxes start to decrease while grounding line and basal melt fluxes continue increasing. As WAIS tips to its deglaciated state (transition to purple shading), all fluxes decrease sharply in response to the reduction in ice sheet extent. In the deglaciated WAIS state and during subsequent tipping back to a glaciated state, grounding line and ice shelf basal melt fluxes both decrease as ocean temperature decreases, while calving remains relatively steady.

the only recent interglacial in which the 0 to +0.25 °C warming threshold was crossed for insufficient duration to trigger tipping.

Second, we find that tipping of West Antarctica is always initiated in the Amundsen Sea and Weddell Sea sectors, resulting in collapse of the divide between these basins (Supplementary Videos 1 and 2). Thus, with reference to our first point we consider this as a critical region where tipping is first triggered, consistent with some studies[15,33,63] but not all[17,55].

Third, through the last eight glacial cycles we find negligible retreat of marine or grounded sectors of East Antarctica (the former are considered vulnerable in some studies[49,50])—in both the transient and equilibrium states (Fig. 4). Hence, these regions appear robust to at least ~2 °C ocean warming, consistent with other recent paleo ice sheet simulations[15,17–19,64] except one conceptual experiment employing an increased sensitivity to ice shelf basal melting[50]. However, we note that the high (Shared Socioeconomic Pathway 5-8.5) IPCC warming scenario will surpass ~2 °C deep ocean warming and indeed the ocean warming magnitudes reconstructed in any Quaternary interglacial[54].

Fully coupled Earth-ice-ocean-atmosphere simulations are the ideal tool for investigating this problem further, but at adequate spatial resolution they remain far out of reach at such long time scales. For now, uncoupled ice sheet modelling continues to be a valuable alternative tool that provides a long-term paleo perspective on future climate and sea-level projections. Nevertheless, given the strong dependence on ocean temperature changes, obtaining additional and higher-resolution circumpolar deep water (CDW) temperature reconstructions, and development of proxies to estimate cross-shelf CDW transport under past climate states, should be as high a priority as improving our representation of ice dynamics in future efforts to better constrain our proximity to the onset of irreversible ice loss from Antarctica.

Methods

Solid Earth–ice sheet–ocean–climate interactions on many time scales[40] are a major challenge for ice sheet simulations. Climate, ocean and sea-level forcings in uncoupled ice sheet models are themselves dependent on the simulated ice sheet response, yet the high computational cost of coupled models currently limits experiments to short time periods or coarse spatial resolution[65–68]. Glacial-cycle simulations with adequate representation of grounding line and ice stream dynamics still require uncoupled ice sheet models. However, the missing feedbacks in this uncoupled approach do not necessarily compromise our assessment of ice sheet stability close to present-day conditions, as discussed in the main text.

Our implementation of the PISM ice sheet model and its parameterisations are described in the following sections.

Deep water temperature reconstructions

Ocean temperature is a crucial boundary condition for ice sheet simulations, as ice shelf basal melt contributes about one half[69–71] to two-thirds[72] of present-day ice discharge from Antarctica.

Basal melt is driven by CDW entering sub-shelf cavities at depth (typically 400–1000 m)[73–77], and by high-salinity shelf water (HSSW). As

such, it is the thermal forcing of these water masses—not the sea surface temperature—that we require as a boundary condition. At glacial cycle timescales there are no reconstructions of ocean temperature on the Antarctic continental shelf, and insufficient reconstructions in the Southern Ocean[78–80] with which to force an ice sheet model directly[27,28]. Previous ice sheet simulations over multiple glacial cycles have employed various alternatives to overcome this problem[16–19,25,81], none of which has been validated by comparison with additional paleotemperature reconstructions.

Here we use deep water temperature anomalies estimated with a linear response function (LRF)[25,26]. The LRF assumes that deep ocean temperature responds with a delay and reduced magnitude to changes in global mean surface temperature. This is physically reasonable, as most ocean heat sources and sinks are near the surface, so that changes in deep water temperature must have propagated downwards from preceding surface changes. The delay and damping arise as we would expect from an advective-diffusive system. In the Southern Ocean, surface and deep water temperatures appear well correlated, at least at millennial time scales[27,82]. The LRF has two parameters (response time and damping factor) determined from a 6 kyr ECHAM5-MPIOM $4 \times CO_2$ equilibrium simulation[83] under the assumption that Antarctic surface air temperature scales linearly with global mean temperature (as supported by proxy reconstructions[84]).

The LRF has the distinct advantage of employing ice sheet air temperature reconstructions, which are available at much higher resolution and show stronger inter-site agreement than reconstructions of deep water temperature[23,24,27] or sea surface temperature[82]. Nevertheless, there are some important weaknesses to consider. First, the two LRF parameters from Albrecht et al.[25] are based on one climate model experiment, for warming above present-day conditions. Potentially different response characteristics during cooling below present-day or during warming from glacial climates, were not considered. Second, the method cannot capture changes in stratification or circulation associated with changes in ice discharge[6,61] or ice sheet extent[85]. Third, the response time and scaling factor are constants; accordingly, the same ocean temperature *anomaly* time series is applied to all ice shelves, with spatial variability captured only in the present-day reference temperature.

To address the above three weaknesses we first make an additional comparison with Fast Ocean-Atmosphere Model (FOAM, 1.4° lat × 2.8° lon) simulations[86], which included both cooling and warming after halving or doubling CO_2. In those experiments the equilibrium response times in the Southern Ocean at 65°S would average several hundred years over the depth range 500–2500 m (Fig. 2 in ref. 86). However, if considering CDW at 500 to 1000 m depth (and still 65°S), response times are shorter: ~150–400 years for warming and 150–200 years for cooling[86]. Response times were relatively longer in the Atlantic sector (400 to 450 years warming, 150 to 350 years cooling). This cold-warm asymmetry is common to several models and is likely related to a respective increase or decrease in the strength of meridional overturning associated with cooling or warming[86–88]. While $\tau_r = 500$ yr is thus a reasonable estimate for warming in the deep ocean, a shorter $\tau_r \sim 200$ yr could be argued to better represent warming and cooling of Southern Ocean CDW. However, neither the FOAM[86] nor the ECHAM5-MPIOM[83] simulations include ice-ocean feedbacks or small-scale processes, that could locally modify these response times. Therefore, we have continued to use $\tau_r = 500$ yr for consistency with Albrecht et al.[25].

Changes in ocean circulation could impact access of warm water masses to sub-shelf cavities. In the 'cold' Filchner-Ronne and Ross ice shelves, sub-shelf melting near the grounding line is likely driven by HSSW rather than CDW *at present*. Thus, our CDW temperature anomaly approach may be less appropriate for those two shelves. However, even beneath Filchner-Ronne, there is some on-shelf transport of warm water masses (Weddell Deep Water)[89,90].

In East Antarctica, most ice shelves were classified as cold ('fresh' or 'dense': ref. 91), but observations increasingly point to the importance of CDW intrusions in several key regions[74,76,77,92]. Hence, changes in offshore CDW temperature should be transmitted to water masses within ice shelf cavities, to some extent, under a present-day climate state.

In our simulations, we find WAIS collapse occurs close to present-day conditions, when uncertainties in water mass or temperature *changes* from present-day observations are small. This should limit the sensitivity of our stability assessment to oceanographic circulation changes, in particular with regard to cross-shelf transport of CDW.

The lack of validation of our LRF-based ocean temperature anomaly is addressed by comparison with a CDW temperature reconstruction[27,28] (Fig. S1). Despite the two temperature estimates having important but independent uncertainties (Methods and ref. 27), we find encouraging agreement when the LRF is resampled to the same 4 kyr resolution as the reconstructions (Fig. S1). Evidently colder temperature anomalies in the LRF than in the proxy reconstruction during glacial periods may be explained by very cold surface air temperatures being propagated through the LRF. However, PISM ocean temperatures are bounded below by the freezing point (~−1.8 °C), so in practice the glacial temperature anomalies used by PISM will be warmer than shown here (depending on the PICO basin), hence the discrepancy between the LRF and proxy record is less marked than would first appear.

In summary we consider that the LRF represents the changes in deep ocean temperature at glacial-interglacial time scales reasonably well, but its ability to capture shorter (<~1 kyr) time-scale variability cannot yet be evaluated as deep water temperature proxy records[27] have insufficient temporal resolution to enable detailed comparison.

Present-day deep water temperature

Deep water temperatures imposed as anomalies from the present-day require a modern reference. Three existing possibilities are the Schmidtko et al.[34] shelf bottom water temperature dataset as already used in PISM simulations[25,55,93]; the 2018 World Ocean Atlas (WOA2018)[94] which includes many additional observations close to ice fronts; or a temperature dataset compiled using WOA2018 and a spatial interpolation/extrapolation algorithm[95] for the Ice Sheet Model Intercomparison Project phase 6 (ISMIP6)[96].

WOA2018 reports two temperatures. First is the statistical mean, only in grid boxes with observed conductivity-temperature-depth profiles. These are relatively sparsely distributed around Antarctica. Second is the objectively analysed mean, for all ocean grid boxes after filling data gaps with an extrapolation and interpolation algorithm. When applied to sparse data around Antarctica, both the WOA2018[94] and ISMIP6[95] extrapolation routines can transfer water temperatures horizontally from distant regions where the water is much deeper. Therefore, both algorithms could misrepresent bottom water temperatures where upwelling CDW follows isopycnals that slope upwards towards the continental shelf[97,98]. Since we only need a single temperature for each PICO basin, rather than a gridded temperature field, we use a simpler method that avoids some potential pitfalls from extrapolation, in two steps as follows. (1) If the seafloor depth is between 500 and 800 m, we return the average of the statistically analysed mean temperatures—where available—at levels within 100 m of the seafloor. If there are no such temperatures we return an invalid temperature for that grid cell. Noting that the continental shelf depth is typically at 400 m around Antarctica (Fig. S3b), the choice of 500–800 m is based on present-day depths of CDW that is either (i) upwelling onto the continental shelf, from deeper levels adjacent to the shelf; or (ii) crossing the continental shelf through incised troughs, which have been observed as efficient routes of CDW access to ice shelf cavities[5,99,100]. These troughs are evident in Fig. S3b. The upper limit of 500 m (which is deeper than some regions of the shelf) minimises the influence of outflowing surface waters that have been cooled by contact with the ice shelf; this mainly affects the uppermost ~500 m of the water column[101]. (2) Bottom water temperatures identified in Step 2 are averaged across all valid grid cells in each PICO basin (Fig. S3a). For basins with insufficient data (Fig. S3c), we combine data from that basin with data from an adjacent basin.

Basin-average temperatures calculated by this method are reasonably consistent with basin-averages calculated using the Schmidtko et al. dataset[25,34] (within 0.2 °C).

PISM Ice sheet simulations

We use the Parallel Ice Sheet Model[21,22,102], which includes the Potsdam Ice-shelf Cavity mOdel (PICO)[103], to simulate the Antarctic Ice Sheet over the last eight glacial cycles (800 ka to present). PISM is a 3D ice flow model employing a hybrid shallow-ice/shallow-shelf approximation (SIA/SSA) to the Stokes equations for ice flow[21,22]. The model parameterises other ice sheet processes (surface mass balance, basal friction, grounding line dynamics, calving, ice shelf basal melt, isostatic rebound) to varying degrees of complexity[21,22,25,103–105]. We use the same grid as that used in several recent studies[19,25,55,93] (16 km horizontal resolution; 81 quadratically-spaced vertical layers with smallest Δz near the bed), and the more recent Bedmachine V3 bed topography[1]. This horizontal resolution better captures major ice streams than the 40 km resolution more commonly used at these time scales[16,50,81,106]. An increase to 8 km resolution increases computational time by a factor of 10 with no substantial change in simulated ice volume through the last two glacial cycles[25]. However, some small-scale features such as ice shelf pinning-points could potentially be absent at our resolution; these can impart some stability by providing additional buttressing.

Detailed studies of the PISM parameter sensitivities have already recommended optimal model choices[25,93,107]. Since these studies achieved reasonable present-day ice sheet states we start by following their broad recommendations, but with modifications motivated or forced by additional constraints as follows. (1) We apply a correction to the pressure melting point of seawater in ice-shelf cavities as described below ("Ice shelf basal melt"). (2) The driving stress gradient at the grounding line is calculated using centred derivatives of the ice thickness, following ref. 33. (3) We use a lower limit on till effective pressure and a higher till friction angle than those used by ref. 25, for closer consistency with the few relevant measurements of till properties[108–111]. We also use PISM's native bed elevation-based till friction angle (ϕ) parameterisation (topg-to-phi) instead of an inversion/optimisation approach—partly to avoid over-fitting one parameter[112], and partly to avoid the problem of assigning ϕ beyond the present-day grounded ice extent.

Due to the many ice sheet and climate parameters that remain poorly constrained[25,93,107], a systematic search of the full parameter space was not computationally feasible even after restricting ranges based on these previous studies. Instead, we used a heuristic approach combining latin hypercube sampling[113] of reduced parameter sets, and ad-hoc testing, in shorter (220 and 33 kyr) simulations to identify model choices that lead to: (1) A reasonable representation of the present-day ice sheet in terms of its grounded and floating ice extents, total ice volume, grounding line flux, and partitioning between calving and basal melting (Fig. S4). (2) A last interglacial ice sheet with lower sea level equivalent ice volume than the present-day ice sheet, to satisfy constraints from sea-level reconstructions (ca. 3 to 7 m SLE smaller[29,53,114–116]. Since there is uncertainty in geological archives regarding the spatial distribution of interglacial ice loss, e.g. the extent of WAIS collapse[13,36,37,40–43,45] and the amount of retreat in EAIS (particularly the Wilkes basin[15,49,51,52])—as noted in the main text—the total sea-level contribution in the last interglacial was used as a tuning target, and not the spatial pattern. In practice we found that all simulations yielding a reasonable present-day ice sheet showed negligible retreat of Wilkes.

Although we could also have considered Last Glacial Maximum (LGM) and Penultimate Glacial Maximum (PGM) ice volumes, these are more uncertain owing to the difficulties in separating the individual contributions of four major ice sheets during glacial periods. However, there are reasonably confident LGM ice extent reconstructions at a few localities along the Bellingshausen and Amundsen Sea shelf breaks and near the Amery Ice Shelf[117,118]. As our anomaly-based forcings become less reliable in increasingly colder climates owing (for example) to likely ocean and atmosphere circulation changes that are not captured, matching these LGM reconstructions was a lower priority. Consequently, our simulated LGM extents (Supplementary Videos 1 and 2) are less advanced than the reconstructions[117,118]. This is likely a conservative outcome: had we continued optimisation to find acceptable configurations that advanced further in the LGM, those configurations would necessarily have needed to lose more ice from LGM to present (to avoid overestimating present-day extent) and similarly from the PGM to Last Interglacial (to ensure WAIS collapse). Hence, those choices would be biased towards dynamic configurations more prone to rapid ice loss, than the configurations A-C used here. Our underestimate of LGM ice advance should be noted as an important discrepancy if interpreting our results with regard to colder climates. However, while glacial ice volume varies across the three model configurations A-C, we note that subsequent interglacial evolution is very consistent (Fig. S1).

Iterative rounds of optimisation led to the three configurations (A, B, C) summarised in Table 1. These yield similar responses to the boundary conditions, with the main difference of note being in the glacial ice volume (Fig. S1). Ice volume anomalies through the interglacials 11, 9, 7, 5 and 1 are remarkably similar.

Grounded ice dynamics

The hybrid SIA/SSA scheme for ice flow is described in detail elsewhere[21,22,102]. Ice creep is modelled by a Glen–Paterson–Budd–Lliboutry–Duval flow law, with spatially uniform enhancement factors (one each for the SIA and SSA)[119]. A pseudo-plastic till friction law[21,120,121] is implemented even though friction in some regions is likely controlled by till-free bedrock, because the most dynamic regions (e.g. ice streams) are underlain by till[122,123]. Spatial variability in till strength is modelled by heuristically specifying a bed elevation-dependent till friction angle (the PISM topg-to-phi parameterisation)[124]. Temporal changes in friction are modelled by tracking changes in till water content with a local, non-conservative water budget[21]. A sub-grid-scale grounding line parameterisation scheme[125,126] provides a reasonable representation of grounding line dynamics (in comparison to a full-Stokes model) even at 16 km grid resolution[126].

Feedbacks between surface melting, hydrology and ice dynamics are not included in our model. Surface melting is currently insufficient over most of the grounded ice in Antarctica to drive supraglacial (and thus subglacial) seasonal hydrological evolution similar to that in Greenland[57,127,128], but future modelling efforts should seek to assess its potential contribution under warmer climates.

Ice shelf basal melt

Ice-ocean interaction is simulated via parameterisations of sub-shelf melting/refreezing and iceberg calving, which are the currently the dominant processes contributing to ice loss from Antarctica[69–71].

Sub-shelf melting is estimated using the PICO box model[103], which takes deep ocean temperature adjacent to each ice shelf as its input and uses a parameterisation of the subshelf overturning circulation to calculate basal melting. Melt rates calculated by PICO are spatially variable and tuned to fit observations, but also account for temporal changes in both the imposed ocean forcing and the ice shelf geometry. We use the standard 5-box PICO implementation[103], except for one change to the pressure melting point (PMP) calculation. Water temperatures applied as anomalies from present-day observations can yield open ocean temperatures below the PMP. PICO truncates these cold temperatures at the local PMP, i.e., corresponding to the water pressure *at the depth of the ice shelf base*, which is colder than the surface PMP. However, since there is no heat sink that could cool deep inflowing ocean water to a temperature below its surface freezing temperature, we instead use the surface freezing temperature as the lower bound for water temperature at all depths. When applying this change, the lower bound on our ocean temperatures is slightly warmer than that using the original (deeper) PMP, leading to slightly higher basal melt estimates at the deeper grounding lines. This change is particularly noticeable during cold climates, when our modification maintains a slightly positive thermal forcing at grounding lines (thus maintaining ca. 400 Gt/yr ice shelf basal melt even during glacials: Fig. S1), whereas basal melting would have reduced to zero in the standard implementation.

Both PICO parameters C and γ_T^* have been assigned values varying by two orders of magnitude in recent PICO optimisation studies[33,103,129,130]. Since we are using a different present-day ocean temperature dataset (see above) to the previous studies, and have applied a warmer PMP, we optimise the parameters C and γ_T^* again. To do this we run PICO with our present-day ocean temperature and the BedMachine V3 ice geometry[1], to calculate mean basal melt rates for each of the 19 PICO basins. These are compared with observations[131] averaged over the same basins. We use a parameter search in the ranges $0.3 \times 10^{-5} \le \gamma_T^* \le 1.0 \times 10^{-5}$ m s^{-1}, $0.1 \times 10^6 \le C \le 20 \times 10^6$ m^6 kg^{-1} s^{-1} to find pairs that yield a reasonable match to the observations.

Although the continental-scale basal melting is not very sensitive to PICO parameter choices (Fig. S5), individual basins show much greater sensitivity. With just two parameters and no temperature corrections we cannot achieve as good a match as some past studies[33,129], in all 19 basins. Therefore, we prioritise the key marine basins (Filchner-Ronne, Amery, Aurora, Wilkes, Ross and Amundsen). This is justified firstly because the Antarctic Peninsula basins 15–19 have relatively small sea level contribution, and have little influence on the dynamics of WAIS or EAIS. Secondly, the remaining EAIS basins 2–5,7,10–11 are mainly grounded above sea-level and are less sensitive to ocean forcing. Even with this reduced constraint we find inconsistent positive/negative melt rate errors in different basins, for a given (γ_T^*, C) pair (Fig. S5). Given there is no clearly optimal solution, we ran an additional ensemble of PISM simulations from 33 ka to present, which samples parameter pairs lying between the Burgard et al. 50 km tuning[129] and Albrecht et al.[25]. In the same ensemble we also varied the two calving parameters (H_{calv}, K_{calv}: see below) to adjust the ratio between basal melting and calving, and varied the threshold velocity u_0 because some adjustments to grounded ice dynamics are typically needed to compensate for changes in ice shelf processes. Members from this ensemble contributed to the final modelling choices used in transient simulations A to C (Table 1). These choices are close to the Burgard et al.[129] 50 km tuning (Fig. S5).

In contrast to the atmospheric forcing there is no seasonality or noise added to the ocean temperature time series. Future work might consider adding some noise or seasonality, based on observed changes in heat transport into ice shelf cavities at seasonal to inter-annual time scales[101,132,133], since the stochastic noise characteristics as well as the long-term mean forcing (or control parameter) can influence tipping and nonlinear responses[134–136].

Calving

Ice shelf calving is modelled using thickness calving and eigencalving schemes[104,137]. The former option calves all ice below a threshold thickness; the latter option estimates calving rate using the strain rate tensor close to the ice front. These two options are employed simultaneously and contribute one parameter each to the tuning process (thickness threshold H_{calv}, and eigencalving constant K_{calv}).

Global mean sea-level

Global mean sea-level is imposed as a scalar time series independent of the modelled ice sheet volume, ignoring regional steric or gravitational effects. Since we need data at least every few kyr (ideally more frequent during rapid deglaciation) we are restricted to records derived from sediment cores, as coral- or speleothem-derived GMSL records tend to be intermittent[138,139]. Several potentially applicable GMSL reconstructions are available[29,79,140,141] (Fig. S1).

There is no obviously preferable record. We chose not to use the Elderfield et al.[79] benthic paired Mg/Ca - δ^{18}O record because of high-amplitude sea-level fluctuations over short time scales, likely attributed to poor signal-to-noise ratio at a single site. Spratt and Lisiecki[141] offer the advantage of a multi-proxy multi-site approach, but their present-day sea-level bias is +9.0 [−1.2, +20.4] m and the comparatively much lower last interglacial high-stand at +0.4 [−23.5, +14.0] m is inconsistent with other evidence[13,29,142]. The Grant et al.[140] Red Sea record has a lower present-day offset of +1.7 [−4.0, 7.4] m, and higher last interglacial high-stand at +4.7 [+1.6, +7.8] m, and the distinct advantage (for our purposes) of being independent of ice sheet volume, but is missing the period from 800 to 492 ka. However, the missing part of that record can be substituted using a parameterisation of the Antarctic air temperature record which yields an excellent fit after 492 ka (Fig. S1). That parameterisation and the Grant et al.[140] record are reasonably consistent (within the wide errors) of the Spratt and Lisiecki[141] record adjusted for the present-day offset (Fig. S1), as well as with Rohling et al.[29]. Finally, the Rohling et al.[29] re-analysis of the LR04[143] benthic stack and Spratt et al.[141] GMSL yields a GMSL record that is more consistent with other evidence as noted above. Here we used the Grant et al.[140] Red Sea sea-level reconstruction (and its parameterised extension to 800 ka) in our earlier PISM tuning simulations and first transient run (Run A). We used the Rohling et al.[29] LR04 reanalysis in our subsequent PISM tuning and transient runs (Runs B and C).

Glacial isostatic adjustment

We use the PISM implementation of the Lingle-Clark[144] model, comprising an elastic lithosphere overlying a viscous mantle. This includes Earth deformation but not rotational effects; see Albrecht et al.[25] for more details. The spatially uniform mantle viscosity η is treated as a scalar tuning parameter, but since η is spatially variable (by two or more orders of magnitude beneath Antarctica[145]) we prioritise representing the relatively low viscosity beneath the WAIS[146–148]. This decision reflects that the comparatively dynamic WAIS is likely to experience faster changes in ice loading than most regions of East Antarctica. In this respect, isostatic uplift following retreat can impart some stability, by locally reducing relative sea-level[146]. However, by underestimating η beneath East Antarctica, we overestimate GIA uplift rate during retreat, which potentially biases the marine sectors of East Antarctica towards stability[148]. Nevertheless, two previous studies with higher η found WAIS collapse with no additional ocean warming, yet no substantial retreat in East Antarctica (similar to our study): these were Golledge et al.[15] with $\eta = 1.3 \times 10^{20}$ Pa s and Reese et al.[33] with no GIA (effectively an infinite viscosity). Future modelling efforts would benefit from a spatially variable mantle rheology, for example using the recently developed PISM-VILMA coupled model[149].

Surface climate

The present-day surface temperature and precipitation fields follow Albrecht et al.[25], based on ERA-Interim C20[150] (temperature) and RACMO2.3p2[151] (precipitation). Temperature changes are applied as anomalies to present-day values, adjusted for changes in ice surface elevation and air temperature (again following Albrecht et al.[25]). Therefore, some processes are not included: for example, changes in large-scale atmospheric circulation which modify the spatial patterns of temperature and precipitation.

Our surface temperature anomaly uses a five-site average air temperature reconstruction where possible (i.e., after 650 ka)[24,152], and the single-site Dome C (EDC) record from 800 to 655 ka[23]. The Parrenin et al.[24] average comprises EDC throughout[23], and additionally Vostok after 415 ka[153], Dome Fuji after 335 ka[154], Talos Dome (TALDICE) after 247 ka[155], and Dronning Maud Land (EDML) after 140 ka[156]. Hence, the imposed anomaly reflects temperature changes at high-elevation ice divides in East Antarctica. Cores from West Antarctic ice divides do not reach the last interglacial[157,158].

Air temperature thresholds for precipitation phase changes (rain to snow) follow PISM defaults of all rain above 275.15 K; all snow below 273.15 K; and a linear change in between.

The climate forcing contributes one tuning parameter: precipitation scaling factor f_{prec}, which quantifies the decrease in precipitation with temperature to account for the reduced moisture capacity of colder air[25,159,160]. Comparing our three transient runs with f_{prec} set to 5.0%, 4.4% and 6.0% (Fig. S1) we find that glacial ice volume varies by up to 4 mSLE between the three runs, while interglacial ice loss is very consistent

(differences <1 mSLE). This suggests our main result regarding tipping at <0.25 °C ocean warming is not sensitive to f_{prec}. Nevertheless, future development might consider whether f_{prec} should vary temporally through glacial cycles.

Initial state

Our transient simulations start in the glacial MIS 20 (800 ka), when the forcing time series have similar values to those at 140 ka in the penultimate glacial MIS 6 (Fig. 1). Hence, we use a 140 ka snapshot from a suitable optimisation run as the initial state for the full 800 ka simulation. The initial state for the optimisation runs is a 220 ka snapshot from Albrecht et al.[25].

Equilibrium simulations

We start equilibrium simulations from transient Run C snapshots at 235 targeted points in the ocean temperature anomaly time series: these are at present day; at glacial/interglacial peaks; and at temperature thresholds every 0.25 °C from -3 to +1.5 °C. A smaller number focusing on warm climates was selected for Run B, and only the present-day for Run A. Equilibrium runs used identical modelling choices to those of their respective transient run, while the ocean temperature, surface temperature and GMSL forcings were frozen at their respective conditions at the time of the snapshot. We ran all equilibrium simulations for 100 kyr. There was little notable difference in results obtained after 50 and 100 kyr (illustated for Run B in Fig. S6), except in two MIS 9 simulations where onset of the melt-elevation feedback after 60 kyr caused substantial EAIS ice loss that was still ongoing after 100 kyr. This feedback emerged at time scales that are not relevant to future projections or even orbital time scales; hence we use the 50 kyr equilibrium state to avoid the influence of this feedback.

From 40 to 50 kyr, drift in all equilibrium simulations was within ±0.05 m SLE/kyr (and mostly within ±0.02 m SLE/kyr), and the standard deviation was <0.06 m SLE.

Data availability

Links to proxy data are provided in the respective references. Output from the PISM ice sheet model is available at https://ns9999k.webs.sigma2.no/10.11582_2025.00061/.

Code availability

The PISM ice sheet model is freely available at https://www.pism.io/. Notebooks to plot the figures are available at https://ns9999k.webs.sigma2.no/10.11582_2025.00061/.

Received: 21 February 2025; Accepted: 6 May 2025;
Published online: 30 May 2025

References

1. Morlighem, M. et al. Deep glacial troughs and stabilizing ridges unveiled beneath the margins of the Antarctic ice sheet. *Nat. Geosci.* **13**, 132–137 (2020).
2. Fox-Kemper, B. et al. Ocean, cryosphere and sea level change. In: Masson-Delmotte, V. et al. (eds.) *Climate Change 2021: The Physical Science Basis. Contribution of Working Group I to the Sixth Assessment Report of the Intergovernmental Panel on Climate Change* (Cambridge University Press, 2021).
3. Bamber, J. L., Oppenheimer, M., Kopp, R. E., Aspinall, W. P. & Cooke, R. M. Ice sheet and climate processes driving the uncertainty in projections of future sea level rise: findings from a structured expert judgement approach. *Earth's Future* **n/a**, e2022EF002772 (2022).
4. Edwards, T. L. et al. Revisiting Antarctic ice loss due to marine ice-cliff instability. *Nature* **566**, 58–64 (2019).
5. Rintoul, S. R. The global influence of localized dynamics in the Southern Ocean. *Nature* **558**, 209–218 (2018).
6. Mackie, S., Smith, I. J., Stevens, D. P., Ridley, J. K. & Langhorne, P. J. Interactions between Increasing CO_2 and Antarctic melt rates. *J. Clim.* **33**, 8939–8956 (2020).
7. Swart, N. C. et al. The Southern Ocean Freshwater Input from Antarctica (SOFIA) initiative: scientific objectives and experimental design. *Geosci. Model Dev.* **16**, 7289–7309 (2023).
8. Lenton, T. M. et al. Tipping elements in the Earth's climate system. *Proc. Natl. Acad. Sci. U.S.A.* **105**, 1786–1793 (2008).
9. Wunderling, N. et al. Climate tipping point interactions and cascades: a review. *Earth Syst. Dyn.* **15**, 41–74 (2024).
10. Schoof, C. Ice sheet grounding line dynamics: Steady states, stability, and hysteresis. *J. Geophys. Res. Earth Surf.* **112**, F03S28 (2007).
11. Pollard, D., DeConto, R. M. & Alley, R. B. Potential Antarctic Ice Sheet retreat driven by hydrofracturing and ice cliff failure. *Earth Planet. Sci. Lett.* **412**, 112–121 (2015).
12. Thomas, Z. A. et al. Tipping elements and amplified polar warming during the Last Interglacial. *Quat. Sci. Rev.* **233**, 106222 (2020).
13. Turney, C. S. M. et al. Early Last Interglacial ocean warming drove substantial ice mass loss from Antarctica. *Proc. Natl. Acad. Sci. USA* **117**, 3996–4006 (2020).
14. DeConto, R. M. et al. The Paris Climate Agreement and future sea-level rise from Antarctica. *Nature* **593**, 83–89 (2021).
15. Golledge, N. R. et al. Retreat of the Antarctic Ice Sheet during the last interglaciation and implications for future change. *Geophys. Res. Lett.* **48**, e2021GL094513 (2021).
16. Pollard, D. & DeConto, R. M. Description of a hybrid ice sheet-shelf model, and application to Antarctica. *Geosci. Model Dev.* **5**, 1273–1295 (2012).
17. Quiquet, A., Dumas, C., Ritz, C., Peyaud, V. & Roche, D. M. The GRISLI ice sheet model (version 2.0): calibration and validation for multi-millennial changes of the Antarctic ice sheet. *Geosci. Model Dev.* **11**, 5003–5025 (2018).
18. Tigchelaar, M., Timmermann, A., Pollard, D., Friedrich, T. & Heinemann, M. Local insolation changes enhance Antarctic interglacials: insights from an 800,000-year ice sheet simulation with transient climate forcing. *Earth Planet. Sci. Lett.* **495**, 69–78 (2018).
19. Sutter, J. et al. Modelling the Antarctic Ice Sheet across the mid-Pleistocene transition—implications for oldest ice. *Cryosphere* **13**, 2023–2041 (2019).
20. Past Interglacials Working Group of PAGES. Interglacials of the last 800,000 years. *Rev. Geophys.* **54**, 162–219 (2016).
21. Bueler, E. & Brown, J. Shallow shelf approximation as a "sliding law" in a thermomechanically coupled ice sheet model. *J. Geophys. Res. Earth Surf.* **114**, F03008 (2009).
22. Winkelmann, R. et al. The Potsdam Parallel Ice Sheet Model (PISM-PIK)—part 1: model description. *Cryosphere* **5**, 715–726 (2011).
23. Jouzel, J. et al. Orbital and Millennial Antarctic climate variability over the past 800,000 years. *Science* **317**, 793–796 (2007).
24. Parrenin, F. et al. Synchronous change of atmospheric CO_2 and Antarctic temperature during the last deglacial warming. *Science* **339**, 1060–1063 (2013).
25. Albrecht, T., Winkelmann, R. & Levermann, A. Glacial-cycle simulations of the Antarctic Ice Sheet with the Parallel Ice Sheet Model (PISM) – Part 1: boundary conditions and climatic forcing. *Cryosphere* **14**, 599–632 (2020).
26. Winkelmann, R. & Levermann, A. Linear response functions to project contributions to future sea level. *Clim. Dyn.* **40**, 2579–2588 (2013).
27. Chandler, D. M. & Langebroek, P. M. Glacial-interglacial Circumpolar Deep Water temperatures during the last 800 000 years: estimates from a synthesis of bottom water temperature reconstructions. *Clim. Past* **20**, 2055–2080 (2024).
28. Chandler, D. & Langebroek, P. Glacial-interglacial Circumpolar Deep Water temperatures during the last 800,000 years: estimates from a

synthesis of bottom water temperature reconstructions. *Zenodo* https://zenodo.org/records/13253697 (2025).
29. Rohling, E. J. et al. Comparison and synthesis of sea-level and deep-sea temperature variations over the past 40 million years. *Rev. Geophys.* **60**, e2022RG000775 (2022).
30. Rosier, S. H. R. et al. The tipping points and early warning indicators for Pine Island Glacier, West Antarctica. *Cryosphere* **15**, 1501–1516 (2021).
31. Kim, S. et al. Late pleistocene paleoceanographic changes in the Ross Sea—Glacial-interglacial variations in paleoproductivity, nutrient utilization, and deep-water formation. *Quat. Sci. Rev.* **239**, 106356 (2020).
32. Hill, E. A. et al. The stability of present-day Antarctic grounding lines —Part 1: No indication of marine ice sheet instability in the current geometry. *Cryosphere* **17**, 3739–3759 (2023).
33. Reese, R. et al. The stability of present-day Antarctic grounding lines —Part 2: onset of irreversible retreat of Amundsen Sea glaciers under current climate on centennial timescales cannot be excluded. *Cryosphere* **17**, 3761–3783 (2023).
34. Schmidtko, S., Heywood, K. J., Thompson, A. F. & Aoki, S. Multidecadal warming of Antarctic waters. *Science* **346**, 1227–1231 (2014).
35. Auger, M., Morrow, R., Kestenare, E., Sallée, J.-B. & Cowley, R. Southern Ocean in-situ temperature trends over 25 years emerge from interannual variability. *Nat. Commun.* **12**, 1–9 (2021).
36. Scherer, R. P. et al. Pleistocene collapse of the West Antarctic Ice Sheet. *Science* **281**, 82–85 (1998).
37. Hillenbrand, C.-D., Fütterer, D. K., Grobe, H. & Frederichs, T. No evidence for a Pleistocene collapse of the West Antarctic Ice Sheet from continental margin sediments recovered in the Amundsen Sea. *Geo-Mar. Lett.* **22**, 51–59 (2002).
38. McKay, R. et al. Pleistocene variability of Antarctic Ice Sheet extent in the Ross Embayment. *Quat. Sci. Rev.* **34**, 93–112 (2012).
39. *Expedition 379 Preliminary Report: Amundsen Sea West Antarctic Ice Sheet History*, International Ocean Discovery Program.
40. Noble, T. L. et al. The sensitivity of the Antarctic Ice Sheet to a changing climate: past, present, and future. *Rev. Geophys.* **58**, e2019RG000663 (2020).
41. Carlson, A. E., Beard, B. L., Hatfield, R. G. & Laffin, M. Absence of West Antarctic-sourced silt at ODP site 1096 in the Bellingshausen Sea during the last interglaciation: support for West Antarctic ice-sheet deglaciation. *Quat. Sci. Rev.* **261**, 106939 (2021).
42. Steig, E. J. et al. Influence of West Antarctic Ice Sheet collapse on Antarctic surface climate. *Geophys. Res. Lett.* **42**, 4862–4868 (2015).
43. Dütsch, M., Steig, E. J., Blossey, P. N. & Pauling, A. G. Response of water isotopes in precipitation to a collapse of the West Antarctic Ice Sheet in high-resolution simulations with the weather research and forecasting model. *J. Clim.* **36**, 5417–5430 (2023).
44. Zou, H., Sime, L. C., Bertler, N. A. N., Keller, E. D. & Wolff, E. W. Plausible last interglacial Antarctic Ice Sheet changes do not fully explain antarctic ice core water isotope records. *Geophys. Res. Lett.* **52**, e2024GL110657 (2025).
45. Lau, S. C. Y. et al. Genomic evidence for West Antarctic Ice Sheet collapse during the Last Interglacial. *Science* **382**, 1384–1389 (2023).
46. Wolff, E. W. et al. The Ronne Ice Shelf survived the last interglacial. *Nature* **638**, 133–137 (2025).
47. Cavitte, M. G. P. et al. A detailed radiostratigraphic data set for the central East Antarctic Plateau spanning from the Holocene to the mid-Pleistocene. *Earth Syst. Sci. Data* **13**, 4759–4777 (2021).
48. Cook, C. P. et al. Dynamic behaviour of the East Antarctic ice sheet during Pliocene warmth. *Nat. Geosci.* **6**, 765–769 (2013).
49. Wilson, D. J. et al. Ice loss from the East Antarctic Ice Sheet during late Pleistocene interglacials. *Nature* **561**, 383–386 (2018).
50. Crotti, I. et al. Wilkes subglacial basin ice sheet response to Southern Ocean warming during late Pleistocene interglacials. *Nat. Commun.* **13**, 1–11 (2022).
51. Goursaud, S. et al. Antarctic Ice Sheet elevation impacts on water isotope records during the last interglacial. *Geophys. Res. Lett.* **48**, e2020GL091412 (2021).
52. Sutter, J. et al. Limited retreat of the Wilkes Basin Ice Sheet during the last interglacial. *Geophys. Res. Lett.* **47**, e2020GL088131 (2020).
53. Barnett, R. L. et al. Constraining the contribution of the Antarctic Ice Sheet to Last Interglacial sea level. *Sci. Adv*. **9**, eadf0198 (2023).
54. Arias, P. et al. Technical summary. In Masson-Delmotte, V. *et al*. (eds.) *Climate Change 2021: The Physical Science Basis. Contribution of Working Group I to the Sixth Assessment Report of the Intergovernmental Panel on Climate Change*, 33–144 (Cambridge University Press, 2021).
55. Garbe, J., Albrecht, T., Levermann, A., Donges, J. F. & Winkelmann, R. The hysteresis of the Antarctic Ice Sheet. *Nature* **585**, 538–544 (2020).
56. Willis, I. C. Intra-annual variations in glacier motion: a review. *Prog. Phys. Geogr. Earth Environ.* **19**, 61–106 (1995).
57. Nienow, P. W., Sole, A. J., Slater, D. A. & Cowton, T. R. Recent advances in our understanding of the role of meltwater in the Greenland Ice Sheet System. *Curr. Clim. Change Rep.* **3**, 330–344 (2017).
58. Phillips, T., Rajaram, H. & Steffen, K. Cryo-hydrologic warming: a potential mechanism for rapid thermal response of ice sheets. *Geophys. Res. Lett*. **37**, L20503 (2010).
59. Chandler, D. M. & Hubbard, A. Widespread partial-depth hydrofractures in ice sheets driven by supraglacial streams. *Nat. Geosci.* **16**, 605–611 (2023).
60. Wallis, B. J., Hogg, A. E., van Wessem, J. M., Davison, B. J. & van den Broeke, M. R. Widespread seasonal speed-up of west Antarctic Peninsula glaciers from 2014 to 2021. *Nat. Geosci.* **16**, 231–237 (2023).
61. Si, Y., Stewart, A. L. & Eisenman, I. Heat transport across the Antarctic Slope Front controlled by cross-slope salinity gradients. *Sci. Adv.* **9**, eadd7049 (2023).
62. Arthern, R. J. & Williams, C. R. The sensitivity of West Antarctica to the submarine melting feedback. *Geophys. Res. Lett.* **44**, 2352–2359 (2017).
63. van den Akker, T. et al. Present-day mass loss rates are a precursor for West Antarctic Ice Sheet collapse. *Cryosphere* **19**, 283–301 (2025).
64. Clark, P. U. et al. Oceanic forcing of penultimate deglacial and last interglacial sea-level rise. *Nature* **577**, 660–664 (2020).
65. Goelzer, H., Huybrechts, P., Loutre, M.-F. & Fichefet, T. Last Interglacial climate and sea-level evolution from a coupled ice sheet–climate model. *Clim. Past* **12**, 2195–2213 (2016).
66. Kreuzer, M. et al. Coupling framework (1.0) for the PISM (1.1.4) ice sheet model and the MOM5 (5.1.0) ocean model via the PICO ice shelf cavity model in an Antarctic domain. *Geosci. Model Dev.* **14**, 3697–3714 (2021).
67. Pelletier, C. et al. PARASO, a circum-Antarctic fully coupled ice-sheet–ocean–sea-ice–atmosphere–land model involving f.ETISh1.7, NEMO3.6, LIM3.6, COSMO5.0 and CLM4.5. *Geosci. Model Dev.* **15**, 553–594 (2022).
68. Siahaan, A. et al. The Antarctic contribution to 21st century sea-level rise predicted by the UK Earth System Model with an interactive ice sheet. *Cryosphere* **16**, 4053–4086 (2021).
69. Depoorter, M. A. et al. Calving fluxes and basal melt rates of Antarctic ice shelves. *Nature* **502**, 89–92 (2013).
70. Rignot, E., Jacobs, S., Mouginot, J. & Scheuchl, B. Ice-shelf melting around Antarctica. *Science* **341**, 266–270 (2013).

71. Davison, B. et al. Annual estimates of basal melting and calving from Antarctic ice shelves during 2010-2019. *Copernicus Meetings* (2022).
72. Liu, Y. et al. Ocean-driven thinning enhances iceberg calving and retreat of Antarctic ice shelves. *Proc. Natl. Acad. Sci. U.S.A.* **112**, 3263–3268 (2015).
73. Walker, D. P. et al. Oceanic heat transport onto the Amundsen Sea shelf through a submarine glacial trough. *Geophys. Res. Lett*. **34**, L02602 (2007).
74. Herraiz-Borreguero, L. et al. Circulation of modified Circumpolar Deep Water and basal melt beneath the Amery Ice Shelf, East Antarctica. *J. Geophys. Res. Oceans* **120**, 3098–3112 (2015).
75. Silvano, A., Rintoul, S. R., Peña-Molino, B. & Williams, G. D. Distribution of water masses and meltwater on the continental shelf near the Totten and Moscow University ice shelves. *J. Geophys. Res. Oceans* **122**, 2050–2068 (2017).
76. Hirano, D. et al. On-shelf circulation of warm water toward the Totten Ice Shelf in East Antarctica. *Nat. Commun.* **14**, 1–15 (2023).
77. Donda, F. et al. Footprint of sustained poleward warm water flow within East Antarctic submarine canyons. *Nat. Commun.* **15**, 1–10 (2024).
78. Hodell, D. A., Venz, K. A., Charles, C. D. & Ninnemann, U. S. Pleistocene vertical carbon isotope and carbonate gradients in the South Atlantic sector of the Southern Ocean. *Geochem. Geophys. Geosyst.* **4**, 1–19 (2003).
79. Elderfield, H. et al. Evolution of ocean temperature and ice volume through the mid-pleistocene climate transition. *Science* **337**, 704–709 (2012).
80. Hasenfratz, A. P. et al. The residence time of Southern Ocean surface waters and the 100,000-year ice age cycle. *Science* **363**, 1080–1084 (2019).
81. Berends, C. J., de Boer, B. & van de Wal, R. S. W. Reconstructing the evolution of ice sheets, sea level, and atmospheric CO_2 during the past 3.6 million years. *Clim. Past* **17**, 361–377 (2021).
82. Chandler, D. & Langebroek, P. Southern Ocean sea surface temperature synthesis: Part 2. Penultimate glacial and last interglacial. *Quat. Sci. Rev.* **271**, 107190 (2021).
83. Li, C., von Storch, J.-S. & Marotzke, J. Deep-ocean heat uptake and equilibrium climate response. *Clim. Dyn.* **40**, 1071–1086 (2013).
84. Shakun, J. D., Lea, D. W., Lisiecki, L. E. & Raymo, M. E. An 800-kyr record of global surface ocean δ18O and implications for ice volume-temperature coupling. *Earth Planet. Sci. Lett.* **426**, 58–68 (2015).
85. De Rydt, J. & Naughten, K. Geometric amplification and suppression of ice-shelf basal melt in West Antarctica. *Cryosphere* **18**, 1863–1888 (2024).
86. Yang, H. & Zhu, J. Equilibrium thermal response timescale of global oceans. *Geophys. Res. Lett*. **38**, L14711 (2011).
87. Gough, W. A. & Lin, C. A. The response of an ocean general circulation model to long time-scale surface temperature anomalies. *Atmos. Ocean* **30**, 653–674 (1992).
88. Li, Q., Luo, Y. & Liu, F. Asymmetric responses of the meridional ocean heat transport to climate warming and cooling in CESM. *Clim. Dyn.* **58**, 961–979 (2022).
89. Morrison, A. K., Hogg, A. MCC., England, M. H. & Spence, P. Warm Circumpolar Deep Water transport toward Antarctica driven by local dense water export in canyons. *Sci. Adv*. **6**, eaav2516 (2020).
90. Darelius, E. et al. Observational evidence for on-shelf heat transport driven by dense water export in the Weddell Sea. *Nat. Commun.* **14**, 1–7 (2023).
91. Thompson, A. F., Stewart, A. L., Spence, P. & Heywood, K. J. The Antarctic slope current in a changing climate. *Rev. Geophys.* **56**, 741–770 (2018).
92. Ribeiro, N. et al. Warm modified circumpolar deep water intrusions drive ice shelf melt and inhibit dense shelf water formation in Vincennes Bay, East Antarctica. *J. Geophys. Res. Oceans* **126**, e2020JC016998 (2021).
93. Albrecht, T., Winkelmann, R. & Levermann, A. Glacial-cycle simulations of the Antarctic Ice Sheet with the Parallel Ice Sheet Model (PISM) – Part 2: parameter ensemble analysis. *Cryosphere* **14**, 633–656 (2020).
94. Locarnini, R. A. et al. World Ocean Atlas 2018, Volume 1: Temperature. In: Mishonov, A. (ed.) *NOAA Atlas NESDIS 81* (NOAA, 2018).
95. Jourdain, N. C. et al. A protocol for calculating basal melt rates in the ISMIP6 Antarctic ice sheet projections. *Cryosphere* **14**, 3111–3134 (2020).
96. Nowicki, S. M. J. et al. Ice Sheet Model Intercomparison Project (ISMIP6) contribution to CMIP6. *Geosci. Model Dev.* **9**, 4521–4545 (2016).
97. Walker, D. P., Jenkins, A., Assmann, K. M., Shoosmith, D. R. & Brandon, M. A. Oceanographic observations at the shelf break of the Amundsen Sea, Antarctica. *J. Geophys. Res. Oceans* **118**, 2906–2918 (2013).
98. Stewart, A. L. & Thompson, A. F. Eddy-mediated transport of warm Circumpolar Deep Water across the Antarctic Shelf Break. *Geophys. Res. Lett.* **42**, 432–440 (2015).
99. Jacobs, S. et al. The Amundsen Sea and the Antarctic Ice Sheet. *Oceanography* **25**. https://www.jstor.org/stable/24861409 (2012).
100. van Wijk, E. M., Rintoul, S. R., Wallace, L. O., Ribeiro, N. & Herraiz-Borreguero, L. Vulnerability of Denman glacier to ocean heat flux revealed by profiling float observations. *Geophys. Res. Lett.* **49**, e2022GL100460 (2022).
101. Yang, H. W. et al. Seasonal variability of ocean circulation near the Dotson Ice Shelf, Antarctica. *Nat. Commun.* **13**, 1–11 (2022).
102. The PISM authors. PISM Parallel Ice Sheet Model (2023). https://www.pism.io. [Online; accessed 3 Apr 2023].
103. Reese, R., Albrecht, T., Mengel, M., Asay-Davis, X. & Winkelmann, R. Antarctic sub-shelf melt rates via PICO. *Cryosphere* **12**, 1969–1985 (2018).
104. Levermann, A. et al. Kinematic first-order calving law implies potential for abrupt ice-shelf retreat. *Cryosphere* **6**, 273–286 (2012).
105. Bueler, E. & van Pelt, W. Mass-conserving subglacial hydrology in the Parallel Ice Sheet Model version 0.6. *Geosci. Model Dev.* **8**, 1613–1635 (2015).
106. de Boer, B., Lourens, L. J. & van de Wal, R. S. W. Persistent 400,000-year variability of Antarctic ice volume and the carbon cycle is revealed throughout the Plio-Pleistocene. *Nat. Commun.* **5**, 1–8 (2014).
107. Phipps, S. J., Roberts, J. L. & King, M. A. An iterative process for efficient optimisation of parameters in geoscientific models: a demonstration using the Parallel Ice Sheet Model (PISM) version 0.7.3. *Geosci. Model Dev.* **14**, 5107–5124 (2021).
108. Tulaczyk, S., Kamb, W. B. & Engelhardt, H. F. Basal mechanics of Ice Stream B, west Antarctica: 1. Till mechanics. *J. Geophys. Res. Solid Earth* **105**, 463–481 (2000).
109. Rathbun, A. P., Marone, C., Alley, R. B. & Anandakrishnan, S. Laboratory study of the frictional rheology of sheared till. *J. Geophys. Res. Earth Surf*. **113**, F02020 (2008).
110. Iverson, N. R. Shear resistance and continuity of subglacial till: hydrology rules. *J. Glaciol.* **56**, 1104–1114 (2010).
111. Zoet, L. K. & Iverson, N. R. A healing mechanism for stick-slip of glaciers. *Geology* **46**, 807–810 (2018).
112. Berends, C. J., van de Wal, R. S. W., van den Akker, T. & Lipscomb, W. H. Compensating errors in inversions for subglacial bed roughness: same steady state, different dynamic response. *Cryosphere* **17**, 1585–1600 (2023).
113. Bouhlel, M. A. et al. A python surrogate modeling framework with derivatives. *Adv. Eng. Softw.* **135**, 102662 (2019).

114. Kopp, R. E., Simons, F. J., Mitrovica, J. X., Maloof, A. C. & Oppenheimer, M. Probabilistic assessment of sea level during the last interglacial stage. *Nature* **462**, 863–867 (2009).
115. Dutton, A. et al. Sea-level rise due to polar ice-sheet mass loss during past warm periods. *Science* **349**, aaa4019 (2015).
116. Dyer, B. et al. Sea-level trends across The Bahamas constrain peak last interglacial ice melt. *Proc. Natl. Acad. Sci. USA* **118**, e2026839118 (2021).
117. Bentley, M. J. et al. A community-based geological reconstruction of Antarctic Ice Sheet deglaciation since the Last Glacial Maximum. *Quat. Sci. Rev.* **100**, 1–9 (2014).
118. Klages, J. P. et al. Limited grounding-line advance onto the West Antarctic continental shelf in the easternmost Amundsen Sea Embayment during the last glacial period. *PLoS One* **12**, e0181593 (2017).
119. Aschwanden, A., Bueler, E., Khroulev, C. & Blatter, H. An enthalpy formulation for glaciers and ice sheets. *J. Glaciol.* **58**, 441–457 (2012).
120. Schoof, C. A variational approach to ice stream flow. *J. Fluid Mech.* **556**, 227–251 (2006).
121. Schoof, C. & Hindmarsh, R. C. A. Thin-film flows with wall slip: an asymptotic analysis of higher order glacier flow models. *Q. J. Mech. Appl. Math.* **63**, 73–114 (2010).
122. Engelhardt, H., Humphrey, N., Kamb, B. & Fahnestock, M. Physical conditions at the base of a fast moving Antarctic ice stream. *Science* **248**, 57–59 (1990).
123. Smith, A. M. Basal conditions on Rutford Ice Stream, West Antarctica, from seismic observations. *J. Geophys. Res. Solid Earth* **102**, 543–552 (1997).
124. Martin, M. A. et al. The Potsdam Parallel Ice Sheet Model (PISM-PIK) —Part 2: dynamic equilibrium simulation of the Antarctic ice sheet. *Cryosphere* **5**, 727–740 (2011).
125. Gladstone, R. M., Payne, A. J. & Cornford, S. L. Parameterising the grounding line in flow-line ice sheet models. *Cryosphere* **4**, 605–619 (2010).
126. Feldmann, J., Albrecht, T., Khroulev, C., Pattyn, F. & Levermann, A. Resolution-dependent performance of grounding line motion in a shallow model compared with a full-Stokes model according to the MISMIP3d intercomparison. *J. Glaciol.* **60**, 353–360 (2014).
127. Bartholomew, I. et al. Seasonal evolution of subglacial drainage and acceleration in a Greenland outlet glacier. *Nat. Geosci.* **3**, 408–411 (2010).
128. Chandler, D. M. et al. Rapid development and persistence of efficient subglacial drainage under 900 m-thick ice in Greenland. *Earth Planet. Sci. Lett.* **566**, 116982 (2021).
129. Burgard, C., Jourdain, N. C., Reese, R., Jenkins, A. & Mathiot, P. An assessment of basal melt parameterisations for Antarctic ice shelves. *Cryosphere* **16**, 4931–4975 (2022).
130. Johnson, A., Aschwanden, A., Albrecht, T. & Hock, R. Range of 21st century ice mass changes in the Filchner-Ronne region of Antarctica. *J. Glaciol*. **69**, 1203–1213 (2023).
131. Adusumilli, S., Fricker, H. A., Medley, B., Padman, L. & Siegfried, M. R. Interannual variations in meltwater input to the Southern Ocean from Antarctic ice shelves. *Nat. Geosci.* **13**, 616–620 (2020).
132. Jendersie, S., Williams, M. J. M., Langhorne, P. J. & Robertson, R. The density-driven winter intensification of the Ross Sea circulation. *J. Geophys. Res. Oceans* **123**, 7702–7724 (2018).
133. Vaňková, I. & Nicholls, K. W. Ocean variability beneath the Filchner-Ronne ice shelf inferred from basal melt rate time series. *J. Geophys. Res. Oceans* **127**, e2022JC018879 (2022).
134. Serletis, A., Shahmoradi, A. & Serletis, D. Effect of noise on the bifurcation behavior of nonlinear dynamical systems. *Chaos, Solitons Fractals* **33**, 914–921 (2007).
135. Niu, L., Lohmann, G. & Gowan, E. J. Climate noise influences ice sheet mean state. *Geophys. Res. Lett.* **46**, 9690–9699 (2019).
136. Robel, A. A., Verjans, V. & Ambelorun, A. A. Biases in ice sheet models from missing noise-induced drift. *Cryosphere* **18**, 2613–2623 (2024).
137. Albrecht, T., Martin, M., Haseloff, M., Winkelmann, R. & Levermann, A. Parameterization for subgrid-scale motion of ice-shelf calving fronts. *Cryosphere* **5**, 35–44 (2011).
138. Hibbert, F. D. et al. Coral indicators of past sea-level change: a global repository of U-series dated benchmarks. *Quat. Sci. Rev.* **145**, 1–56 (2016).
139. Dumitru, O. A., Polyak, V. J., Asmerom, Y. & Onac, B. P. Last interglacial sea-level history from speleothems: a global standardized database. *Earth Syst. Sci. Data* **13**, 2077–2094 (2021).
140. Grant, K. M. et al. Sea-level variability over five glacial cycles. *Nat. Commun.* **5**, 1–9 (2014).
141. Spratt, R. M. & Lisiecki, L. E. A Late Pleistocene sea level stack. *Clim. Past* **12**, 1079–1092 (2016).
142. Lambeck, K., Rouby, H., Purcell, A., Sun, Y. & Sambridge, M. Sea level and global ice volumes from the Last Glacial Maximum to the Holocene. *Proc. Natl. Acad. Sci. USA* **111**, 15296–15303 (2014).
143. Lisiecki, L. E. & Raymo, M. E. A Pliocene-Pleistocene stack of 57 globally distributed benthic δ18O records. *Paleoceanogr. Paleoclimatol.* **20**, PA1003 (2005).
144. Lingle, C. S. & Clark, J. A. A numerical model of interactions between a marine ice sheet and the solid earth: application to a West Antarctic ice stream. *J. Geophys. Res. Oceans* **90**, 1100–1114 (1985).
145. Whitehouse, P. L., Gomez, N., King, M. A. & Wiens, D. A. Solid Earth change and the evolution of the Antarctic Ice Sheet. *Nat. Commun.* **10**, 1–14 (2019).
146. Barletta, V. R. et al. Observed rapid bedrock uplift in Amundsen Sea Embayment promotes ice-sheet stability. *Science* **360**, 1335–1339 (2018).
147. Lowry, D. P. et al. Geologic controls on ice sheet sensitivity to deglacial climate forcing in the Ross Embayment, Antarctica. *Quat. Sci. Adv.* **1**, 100002 (2020).
148. Coulon, V. et al. Contrasting response of West and East Antarctic Ice Sheets to glacial isostatic adjustment. *J. Geophys. Res. Earth Surf.* **126**, e2020JF006003 (2021).
149. Albrecht, T., Bagge, M. & Klemann, V. Feedback mechanisms controlling Antarctic glacial cycle dynamics simulated with a coupled ice sheet–solid Earth model. *Cryosphere* **18**, 4233–4255 (2024).
150. Dee, D. P. et al. The ERA-Interim reanalysis: configuration and performance of the data assimilation system. *Q. J. R. Meteorol. Soc.* **137**, 553–597 (2011).
151. van Wessem, J. M. et al. Modelling the climate and surface mass balance of polar ice sheets using RACMO2 – Part 2: Antarctica (1979–2016). *Cryosphere* **12**, 1479–1498 (2018).
152. Parrenin, F. et al. Antarctic Temperature Stack (ATS) from five different ice cores (EDC, Vostok, Dome Fuji, TALDICE, and EDML). *PANGAEA* (2013).
153. Petit, J. R. et al. Climate and atmospheric history of the past 420,000 years from the Vostok ice core, Antarctica. *Nature* **399**, 429–436 (1999).
154. Watanabe, O. et al. Homogeneous climate variability across East Antarctica over the past three glacial cycles. *Nature* **422**, 509–512 (2003).
155. Stenni, B. et al. Expression of the bipolar see-saw in Antarctic climate records during the last deglaciation. *Nat. Geosci.* **4**, 46–49 (2011).
156. EPICA Community Members. et al. One-to-one coupling of glacial climate variability in Greenland and Antarctica. *Nature* **444**, 195–198 (2006).
157. Johnsen, S. J., Dansgaard, W., Clausen, H. B. & Langway, C. C. Oxygen isotope profiles through the Antarctic and Greenland Ice Sheets. *Nature* **235**, 429–434 (1972).

158. Cuffey, K. M. et al. Deglacial temperature history of West Antarctica. *Proc. Natl. Acad. Sci. USA* **113**, 14249–14254 (2016).
159. Frieler, K. et al. Consistent evidence of increasing Antarctic accumulation with warming. *Nat. Clim. Change* **5**, 348–352 (2015).
160. Nicola, L., Notz, D. & Winkelmann, R. Revisiting temperature sensitivity: how does Antarctic precipitation change with temperature? *Cryosphere*. **17**, 2563–2583 (2023).

Acknowledgements

This project has received funding from the European Union's Horizon 2020 research and innovation programme under grant agreement no. 820575 (TiPACCs). The simulations were performed on resources provided by Sigma2 - the National Infrastructure for High Performance Computing and Data Storage in Norway (project NN9868K). RR was supported by the UKRI Natural Environment Research Council (grant numbers NE/Y001451/1 and NE/Z5033441/1). RW and TA were supported by Ocean Cryosphere Exchanges in ANtarctica: Impacts on Climate and the Earth system, OCEAN ICE, which is funded by the European Union, Horizon Europe Funding Programme for research and innovation under grant number 101060452, https://doi.org/10.3030/101060452. OCEAN ICE contribution no. 25. TA and RW acknowledge funding by the German Research Foundation (DFG) in the framework of the priority programme 'Antarctic Research with comparative investigations in Arctic ice areas' by grants WI4556/2-1 and WI4556/4-1 and in the framework of the PalMod project (FKZ: 01LP1925D and 01LP2305B), supported by the German Federal Ministry of Education and Research (BMBF) as a Research for Sustainability initiative (FONA). Development of PISM is supported by NASA grants 20-CRYO2020-0052 and 80NSSC22K0274 and NSF grant OAC-2118285.

Author contributions

P.L., R.W. and D.C. conceived the study. D.C. carried out ice sheet simulations with support from T.A. and R.R. D.C. wrote the manuscript with contributions from P.L., R.R., T.A., J.G. and R.W.

Funding

Open access funding provided by NORCE Norwegian Research Centre AS.

Competing interests

The authors declare no competing interests.

Additional information

Supplementary information The online version contains supplementary material available at https://doi.org/10.1038/s43247-025-02366-2.

Correspondence and requests for materials should be addressed to David M. Chandler.

Peer review information *Communications Earth & Environment* thanks the anonymous reviewers for their contribution to the peer review of this work. Primary Handling Editor: Alireza Bahadori. A peer review file is available.

Reprints and permissions information is available at http://www.nature.com/reprints

Publisher's note Springer Nature remains neutral with regard to jurisdictional claims in published maps and institutional affiliations.

Open Access This article is licensed under a Creative Commons Attribution 4.0 International License, which permits use, sharing, adaptation, distribution and reproduction in any medium or format, as long as you give appropriate credit to the original author(s) and the source, provide a link to the Creative Commons licence, and indicate if changes were made. The images or other third party material in this article are included in the article's Creative Commons licence, unless indicated otherwise in a credit line to the material. If material is not included in the article's Creative Commons licence and your intended use is not permitted by statutory regulation or exceeds the permitted use, you will need to obtain permission directly from the copyright holder. To view a copy of this licence, visit http://creativecommons.org/licenses/by/4.0/.

© The Author(s) 2025